AD-A092 702 NAVAL RESEARCH LAB WASHINGTON DC F/G 20/14
LASER-EXTINCTION AND HIGH-RESOLUTION ATMOSPHERIC TRANSMISSION M--ETC(U)
NOV 80 J A DOWLING, S T HANLEY, J A CURCIO MIPR-ASL-79-8016
UNCLASSIFIED NRL-8446 NL

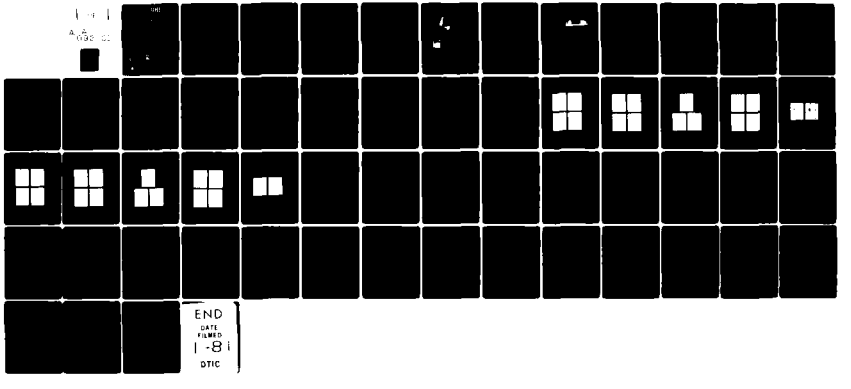

END
DATE FILMED
1-81
DTIC

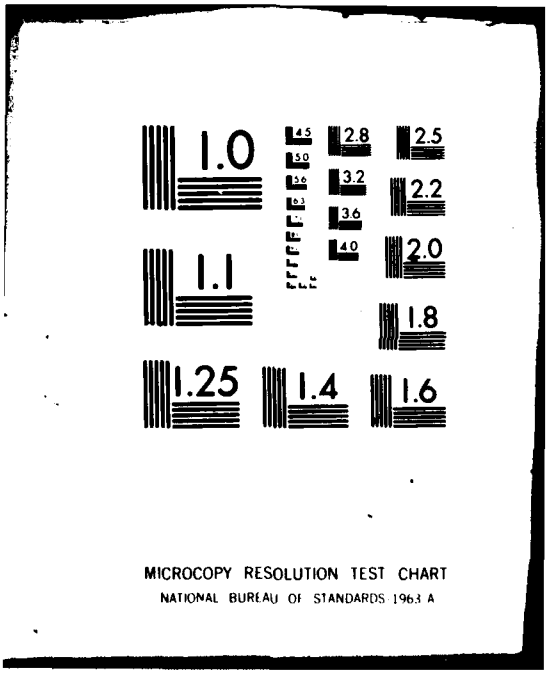
1.0
1.1
1.25
1.4
1.6
1.8
2.0
2.2
2.5
2.8
3.2
3.6
4.0
4.5
5.0
5.6
6.3
MICROCOPY RESOLUTION TEST CHART
NATIONAL BUREAU OF STANDARDS 1963 A

SECURITY CLASSIFICATION OF THIS PAGE (When Data Entered)

REPORT DOCUMENTATION PAGE

READ INSTRUCTIONS BEFORE COMPLETING FORM

1. REPORT NUMBER: NRL Report 8446
2. GOVT ACCESSION NO.: AD-A092 762
3. RECIPIENT'S CATALOG NUMBER:

4. TITLE (and Subtitle): LASER-EXTINCTION AND HIGH-RESOLUTION ATMOSPHERIC TRANSMISSION MEASUREMENTS CONDUCTED AT WHITE SANDS MISSILE RANGE, NEW MEXICO, MARCH 1979
5. TYPE OF REPORT & PERIOD COVERED: Final report
6. PERFORMING ORG. REPORT NUMBER:

7. AUTHOR(s): J. A. Dowling, S. T. Hanley, J. A. Curcio, C. O'Gott, and M. A. Woytko
8. CONTRACT OR GRANT NUMBER(s):

9. PERFORMING ORGANIZATION NAME AND ADDRESS: Naval Research Laboratory, Washington, DC 20375
10. PROGRAM ELEMENT, PROJECT, TASK AREA & WORK UNIT NUMBERS: U.S. Army MIPR — ASL-79-8016

11. CONTROLLING OFFICE NAME AND ADDRESS: Naval Research Laboratory, Washington, DC 20375
12. REPORT DATE: November 30, 1980
13. NUMBER OF PAGES: 56

14. MONITORING AGENCY NAME & ADDRESS (if different from Controlling Office):
15. SECURITY CLASS. (of this report): UNCLASSIFIED
15a. DECLASSIFICATION DOWNGRADING SCHEDULE:

16. DISTRIBUTION STATEMENT (of this Report)

Approved for public release; distribution unlimited.

17. DISTRIBUTION STATEMENT (of the abstract entered in Block 20, if different from Report)

18. SUPPLEMENTARY NOTES

19. KEY WORDS (Continue on reverse side if necessary and identify by block number)

Atmospheric transmission
High-resolution atmospheric spectroscopy
Lasers

20. ABSTRACT (Continue on reverse side if necessary and identify by block number)

Measurements of atmospheric transmission over a 6.4-km path were conducted in March 1979 at White Sands Missile Range (WSMR), New Mexico. A deuterium fluoride (DF) laser and a high-resolution Fourier transform spectrometer (FTS) system were used to generate high-quality transmission spectra of the 6.4-km path accurate to ±3% in absolute transmission. Details of the procedures used and results obtained in the absolute transmission calibration of the spectra are presented. Path integral values for HDO, H_2O, CH_4, and N_2O concentrations have been derived from the spectra and results of this analysis are described. Comparisons of measured DF laser extinction coefficients with calculated

(Continues)

DD FORM 1 JAN 73 1473 EDITION OF 1 NOV 65 IS OBSOLETE
S/N 0102-014-6601

SECURITY CLASSIFICATION OF THIS PAGE (When Data Entered)

SECURITY CLASSIFICATION OF THIS PAGE (When Data Entered)

20. Abstract (Continued)

molecular absorption values are presented which show very small aerosol attenuations, generally <0.02 km^{-1} at DF laser wavelengths. Visibilities measured at 0.55 μm during the course of the experiment generally averaged over 100 km.

SECURITY CLASSIFICATION OF THIS PAGE(When Data Entered)

CONTENTS

1. INTRODUCTION 1

2. EXPERIMENTAL EQUIPMENT AND PROCEDURES 3

3. EXPERIMENTAL RESULTS 5

   3.1 Laser Extinction Measurements 5
   3.2 High-Resolution Fourier Transform Spectroscopy Measurements 7
   3.3 Micrometeorological Measurements 42
   3.4 Visibility Measurements 43

4. COMPARISON OF MEASURED AND CALCULATED TRANSMISSION VALUES 45

5. CONCLUSIONS AND RECOMMENDATIONS 49

6. ACKNOWLEDGMENTS 52

7. REFERENCES 52

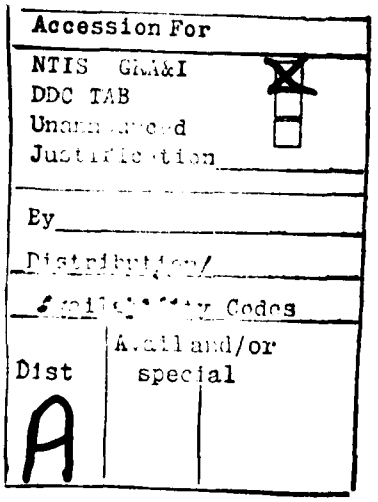

LASER-EXTINCTION AND HIGH-RESOLUTION ATMOSPHERIC TRANSMISSION MEASUREMENTS CONDUCTED AT WHITE SANDS MISSILE RANGE, NEW MEXICO, MARCH 1979

1. INTRODUCTION

This report contains the results of an experiment performed in March 1979 at the White Sands Missile Range (WSMR) by the Optical Radiation Branch of the Naval Research Laboratory. Atmospheric transmission was measured over a 6.4-km path using a low-power deuterium fluoride (DF) laser together with a blackbody infrared source and a high-resolution Fourier transform spectrometer (FTS) system. The portable instrumentation facility used for these measurements is designated the Infrared Mobile Optical Radiation Laboratory (IMORL) and is described in greater detail in Section 2 of this report where additional references are given for further information. Results of the laser extinction and FTS measurements are presented in sections 3.1 and 3.2.

The measurements were performed in the vicinity of the WSMR-MAR site over the same path that was used during a similar experiment carried out in August 1978, described in an earlier report [1]. Figure 1 is a plan view of the area surrounding the 6.4-km optical path extending from a berm near the ARKY site to the PAT site as shown.

Meteorological measurements were performed by the Army Atmospheric Sciences Laboratory (ASL) at the ARKY site during most of the atmospheric transmission measurements. Selected results of the meteorological data are contained in Section 3.3 of this report. Visibility was also measured during the experiment using a telepyrometer technique described in Section 3.4 which also contains a tabulation of the results.

The Army Atmospheric Sciences Laboratory supported the present experiment to complement the infrared propagation data base obtained in August 1978 (as representative of the light wind and relatively moist summer season) with additional data for March as representative of the generally windy and dry spring season. Although in spring it is typically quite dry at WSMR with attendant low molecular absorption by water vapor, occasionally there are high wind conditions accompanied by substantially reduced visibilities due to blowing dust. During the times when long-path measurements documented in this report were performed, the anticipated high wind–low visibility conditions did not materialize. However, such conditions did arise after the IMORL receiver trailer was relocated for post-experiment optical system calibrations (as described in Section 3.1), so that no long-path transmission measurements could be obtained for these conditions.

The data and analyses in this report show that very accurate (±3%) absolute transmission of the atmosphere can be obtained over long atmospheric paths in the high-desert environ-

Manuscript submitted July 28, 1980.

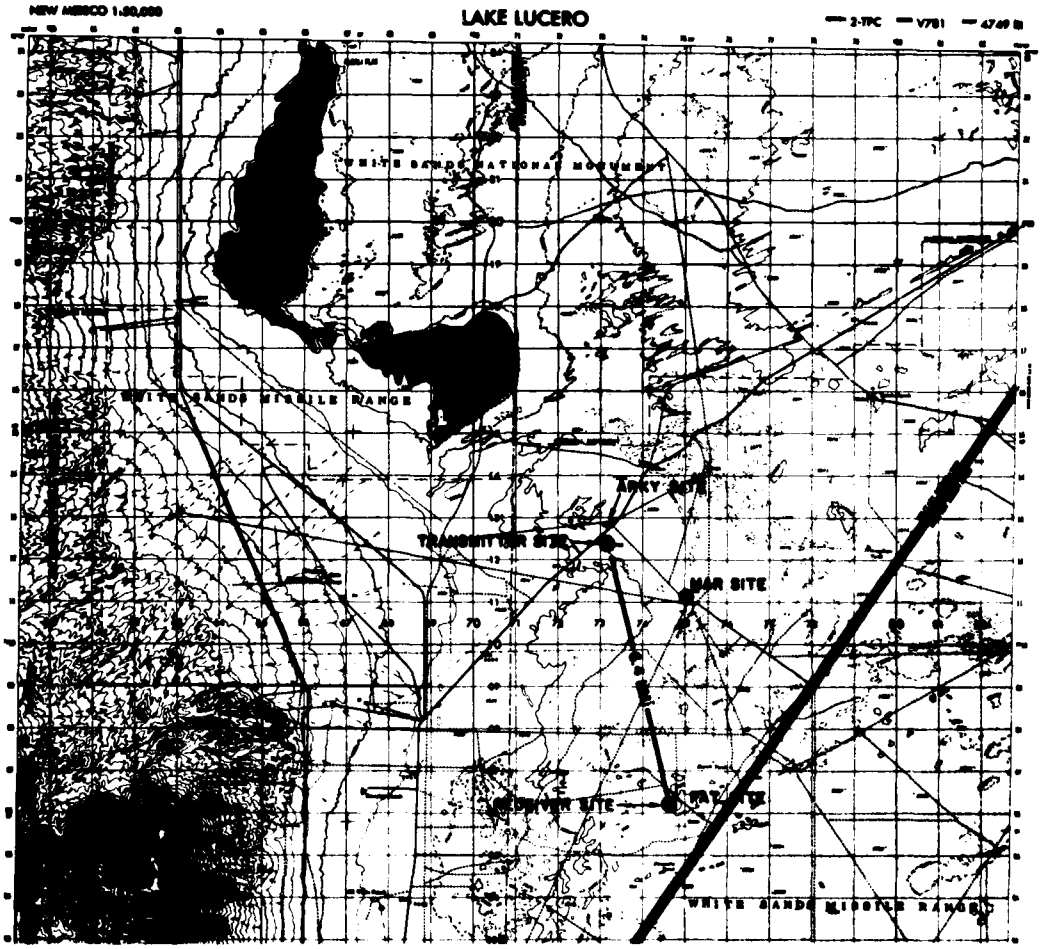

Fig. 1 — Plan view of the optical transmission measurement site at WSMR

ment at WSMR. Absolute transmission calibrations using the large-aperture transmitter and receiver optical systems and single line laser sources, however, must be restricted to those time periods when atmospheric turbulence is minimum; this prevents overfilling the 1.2-m-diameter receiver collecting aperture due to turbulent spreading of the infrared laser beam focused over the long path.

Using the reliable absolute transmission calibrations obtained with the laser extinction measurement system, several high-quality transmission spectra of the 6.4-km path were obtained with spectral resolution sufficient to isolate the individual vibration-rotation line structure of several absorbing molecules in the atmosphere, notably H_2O, HDO, N_2O, and CH_4. Utilization of portions of some of these spectra to extract path average values for concentrations of these absorbers is described in Section 3.2. The analysis presented there is

useful in showing the value of high-resolution long-path spectra to a detailed and thorough understanding of the propagation environment at WSMR.

2. EXPERIMENTAL EQUIPMENT AND PROCEDURES

The IMORL has been developed at NRL as a field laboratory for precision atmospheric propagation measurements. Detailed descriptions of the electro-optical instrumentation contained in the IMORL facility are presented in Ref. 2. Only the essential features of the IMORL system will be reviewed in this report.

The IMORL system has been used extensively to collect laser-calibrated high-resolution atmospheric transmission spectra; it includes several infrared laser and blackbody sources, large, stable telescope optics, a Fourier transform spectrometer (FTS) system, and various support equipment, all of which are transported in and operated from several large semi-trailers. The usual measurement configuration consists of an optical transmitter trailer housing HeNe, Nd-YAG, DF, CO, and CO_2 single-line cw laser sources, relay optics, and a large, stably mounted and precisely pointed, 90-cm-aperture, f/35, Cassegrainian collimating telescope. The small cw combustion-driven DF laser used for much of the laser extinction work requires a large 755 l/s (1600 cfm) vacuum system for operation. This pump is housed in a separate trailer; a 20-cm-diameter vacuum line is installed once the two trailers are properly located at the measurement site. Two additional trailers contain office space, meteorological signal processing and recording electronics, and bottled gas and other consumable supplies used during the course of an experiment.

The FTS system and apparatus used for laser extinction measurements are housed in a receiver trailer which contains a 120-cm-aperture, f/5, Newtonian telescope. The large receiver telescope aperture ensures that the entire laser beam used during long-path (typically 5-km) extinction measurements can be collected, thereby providing reliable absolute transmission calibrations for the FTS measurements. High-resolution transmission spectra are taken by substituting a 1300 K blackbody source for the laser source in the transmitter optical system and adjusting the receiver optical system so as to couple the FTS system to the 120-cm collecting telescope. Repeated calibrations and extensive experience with the measurement system in field experiments have demonstrated that absolute transmission can be reliably measured for long atmospheric paths with an uncertainty less that ±3%.

Figure 2 is a photograph of the transmitter station taken during the experiment at WSMR, with the equipment located at the ARKY hill site [1]. From left to right in the figure can be seen a micrometeorological (met) measurement tower, an office trailer containing met system electronics, a vacuum pump trailer, and an optical transmitter trailer (the 91-cm-aperture telescope mirror and telescope frame may be seen through the open doors).

Figure 3 is a schematic depicting the experimental arrangement used for laser extinction measurements. The output beam from any of the several laser sources used is first collimated by auxiliary optics to a diameter of approximately 18 mm. The beam is then focused via the off-axis parabolic mirror shown in the upper left of Fig. 3 and then diverged to fill the 90-cm transmitter telescope aperture. A 37-Hz, 50%-duty-cycle chopper modulates the beam near the focus formed by the off-axis parabola. The beam is alternately transmitted through the telescope and reflected onto the stationary detector as shown.

Fig. 2 — Photograph of the optical transmitter station near the WSMR — ARKY site

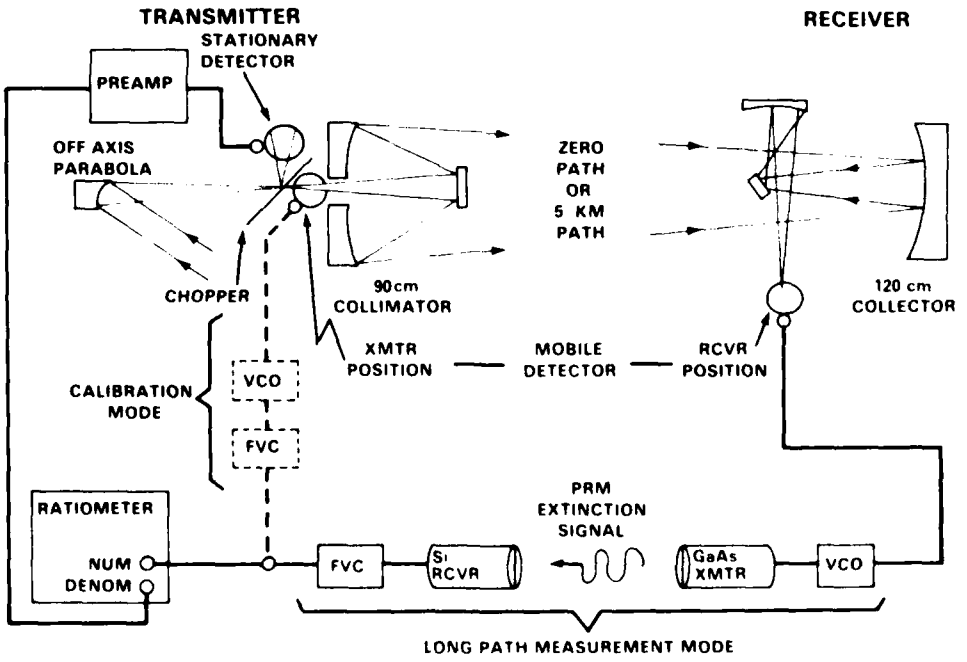

Fig. 3 — Laser extinction measurement schematic

The mobile detector shown in Fig. 3 is placed in the "XMTR" position for calibration measurements in which the relative response of the two detectors is measured. The mobile detector is then placed near the focus of the 120-cm-aperture receiver telescope for (a) calibrations of the large telescope optical efficiencies or (b) long-path extinction measurements. The calibration measurements are carried out with the transmitter and receiver trailers immediately opposite one another, i.e. for $\sim$ zero atmospheric path. When the trailers are separated for long-path measurements, the two types of calibration data are then used to determine absolute atmospheric transmission for the several laser lines studied.

As shown in Fig. 3, the signal produced by the mobile detector in the receiver trailer at one end of the measurement path is relayed to the transmitter by means of a pulse-rate-modulated (PRM) GaAs-laser-based data link. This signal, proportional to laser power at the receiver, is connected to the numerator input of a special-purpose analog ratiometer. The stationary detector signal, proportional to the transmitted laser power, is connected to the denominator input of the ratiometer. Thus, a real-time measure of transmission for the laser line being studied is available at the transmitter site. The ratiometer reading must be corrected for the relative response of the two detectors for that laser line (monitored daily) and the efficiency of the large optical elements beyond the chopper in order to obtain absolute transmission readings. As shown in Fig. 3, the voltage-controlled oscillator (VCO) and frequency-to-voltage converter (FVC) used with the GaAs data link are also connected in the numerator circuit of the ratiometer when the mobile detector is used in the "XMTR" position, so that their combined transfer function is normalized out of the final extinction ratio. Additional information concerning the measurement instrumentation and procedures is contained in Refs. 3 and 4.

Local meteorological measurements of absolute humidity, air temperature, pressure, and windspeed and direction are usually made at each end of the transmission path to (a) document local conditions during a series of measurements, (b) ensure that uniform environmental conditions exist along the measurement path, and (c) ensure that these conditions remain constant during a complete measurement cycle. The period required to make sequential laser extinction and FTS measurements is typically about one hour. Extensive measurements using an aerosol spectrometer system have been performed during some experiments. Infrared aerosol extinction estimates based on Mie scattering calculations utilizing the measured particle distributions have shown good agreement with results derived from infrared extinction measurements at DF laser wavelengths during earlier experiments [4].

3. EXPERIMENTAL RESULTS

3.1 Laser Extinction Measurements

Laser extinction measurements were conducted using the 6.4-km path between the ARKY hill site (transmitter location) and the PAT site (receiver location used for earlier measurements in August 1978 [1]). The average height above ground of the optical line-of-sight varies between 14.6 m (48 ft.) and 17.7 m (58 ft.). A survey of this path is contained in the report of the earlier measurements [1]. Laser extinction measurements were performed on nine days between 8 March and 18 March 1979, and were restricted to DF laser

lines due to malfunctions of the CO_2 laser used for laser extinction measurements near 10 μm. The CO_2 laser problems resulted from damage to the power supply sustained in transit of the transmitter trailer to WSMR from NRL, Washington, D.C. Only one long-path extinction measurement at CO_2 laser wavelengths was possible on 12 March 1979.

Due to optical-turbulence-induced spreading of the laser beam focused over the 6.4-km propagation path, measurements were restricted to periods of minimum optical turbulence. At the ARKY and PAT sites, these periods occur about 80 min after sunrise and 40 min before sunset. Measurements performed in August 1978 occurred predominately in the morning hours (0900-1000). To expand the WSMR transmission data base to include evening conditions, the March measurements in this report were taken during the evening period of low turbulence around 1700 hours.

Table 1 contains a summary of the transmission values measured for the series of lines in the 2 → 1 DF vibrational band available from the cw DF laser source used in the experiment. The P2-8 (2 → 1, P-8) line at 2631.067 cm^{-1} was measured three times during a "run" or measurement sequence to ascertain constancy and repeatability of the transmission measurements. Columns 5 and 6 of Table 1 list the measured transmissions and corresponding extinction coefficients, respectively. The table shows that the measured transmission values are very high with very little loss occurring over the 6.4-km propagation path; the singular exception occurs for the P2-10 DF laser line at 2580.096 cm^{-1} for which the transmission was measured to be between 70% and 80% of that for the lines with consistently high transmission values (P2-8 at 2631.067 cm^{-1} and P2-5 at 2703.999 cm^{-1}).

Zero-path optical system calibration measurements were performed on 20 March 1979 at the ARKY hill site. Very high winds accompanied by dense clouds of blowing sand were experienced at this time. The transmission values observed were significantly (10%) *lower* than the long-path measurements taken during the previous several days and were judged to be inadequate for use in normalizing the long-path measurements using the procedures described in Refs 2 and 4. Additional measurements were scheduled to take place at San Nicolas Island, California, shortly after the data reported here were collected, requiring that the IMORL equipment be transported to that site shortly after the conclusion of the WSMR tests. The optical system used for the measurements in the March 1979 experiment was unchanged from the configuration used in August 1978 and the several reflecting surfaces were in a similar state of cleanliness in each case (cleaned immediately prior to the start of the experiment). Therefore it was determined that the zero-path measurements performed earlier in August 1978 should be used in the reduction of the March 1979 data. The average optical system transmission value of 0.807 ± 0.013 for the DF laser region between 2500 cm^{-1} and 2730 cm^{-1} obtained from the earlier measurements was therefore used to reduce the March 1979 data. This value is consistent with earlier repeated measurements in prior experiments [1,3].

Columns 10 and 11 of Table 1 contain values for calculated molecular absorption (CMA) and differences between measured extinction and CMA values based on the values listed in Column 6 (α) of the table. These differences are discussed in Section 4 of this report.

3.2 High Resolution Fourier Transform Spectroscopy Measurements

3.2.1 Absolute Transmission Calibration

A total of 26 high resolution spectra were measured during the period of 14-21 March 1979.

Hardware problems experienced with the FTS system computer prevented its operation in coincidence with the earlier laser extinction measurements during 8-13 March. Table 2 contains a summary of the FTS measurement times, FTS detector/beamsplitter configurations used (determining wavelength range covered), and the corresponding laser extinction measurement times used for absolute transmission normalization of the FTS spectra. Column 8 of Table 2 lists the designations assigned to the ratioed (R) and normalized (N) spectra obtained in the experiment. The spectra acquired over the 6.4-km path were first ratioed to a spectrum obtained using a local source (i.e. one located approximately 3 m from the FTS instrument) inserted into the FTS telescope optical train. The color temperature of the local source was adjusted to match that of the distant source located in the transmitter trailer by monitoring each with an optical pyrometer. Spectra ASL02, ASL07, ASL08, and ASL16 were taken using the local source.

By ratioing the long-path spectra to local source spectra, the source, beamsplitter, and detector response functions were removed from the resulting spectra. The ratioed spectra were then converted from relative to absolute transmission by determining the scale factor needed to convert the relative transmission value of a spectrum at a particular laser frequency to the absolute transmission value obtained by means of the independent long-path laser extinction measurement. Column 7 of Table 2 lists the time of the laser extinction measurements used for absolute transmission normalization of the several spectra obtained in the experiment. Only long-path spectra which were obtained within one hour of a series of laser extinction measurements were so normalized and are listed in Column 8 of Table 2.

Operation of the FTS system was possible only after 13 March due to data system malfunctions experienced prior to that time. Long-path spectra normalized for absolute transmission by concurrent laser extinction measurements were measured on four days as shown in Table 2, namely 14 and 16-18 March 1979. Attempts to utilize the HgCdTe/KBr detector/beamsplitter combination to collect long-wavelength transmission spectra (6-12 μm) were made on 15 March; however, detector-preamplifier circuit problems were experienced with the result that no satisfactory spectra could be obtained.

Accordingly, the FTS system was reconfigured with the InSb/CaF_2 detector/beamsplitter combination used initially on 14 March, and this was retained for the remainder of the measurements.

Detailed comparisons of the amplitude of each normalized spectrum with the individual DF laser line transmission measurements used to generate the normalization are contained in Table 3 for each of the spectra labeled with an "N" suffix listed in Column 8 of Table 2. An average multiplicative factor was determined by averaging the individual factors obtained for the several laser transmission measurements in any particular measurement series. The laser line identification and position in cm^{-1} are listed in Columns 1 and 2,

Table 1 — Laser Extinction Measurements and Calculated Molecular Absorption

Date	Local Time	Laser Line	ν (cm^{-1})	T	α (km^{-1})	Air Temp (°C)	Barometric Press. (mb)	ppH_2O (Torr)	CMA (km^{-1})	DIFF α-CMA (km^{-1})
3-8-79	1652	P2-8	2631.067	0.963	0.0059	25.0	879	2.0	0.010	-0.004
	53	P2-7	2655.863	0.916	0.0137				0.017	-0.003
	54	P2-6	2680.179	0.941	0.0095				0.012	-0.002
	56	P2-5	2703.999	0.954	0.0074				0.008	-0.001
	59	P2-8	2631.067	0.947	0.0085				0.010	-0.002
	1701	P2-9	2605.806	0.920	0.0130				0.011	0.002
	04	P2-10	2580.096	0.681	0.0600				0.049	0.011
	06	P2-8	2631.067	0.920	0.0130				0.010	0.003
3-9-79	1613	P2-8	2631.067	0.931	0.0112	20.0	880	3.5	0.015	-0.006
	15	P2-7	2655.863	0.852	0.0250				0.029	-0.004
	16	P2-6	2680.179	0.898	0.0168				0.022	-0.005
	17	P2-5	2703.999	0.942	0.0093				0.015	-0.006
	19	P2-4	2727.309	0.908	0.0151				0.021	-0.006
	20	P2-8	2631.067	0.914	0.0141				0.015	-0.001
	22	P2-9	2605.806	0.883	0.0194				0.017	0.002
	29	P2-10	2580.096	0.678	0.0607				0.053	0.007
	30	P2-11	2553.952	0.857	0.0241				0.022	0.002
	32	P2-12	2527.391	0.891	0.0180				0.021	-0.003
	34	P2-8	2631.067	0.925	0.0122				0.015	-0.003
3-12-79	1646	P2-8	2631.067	0.836	0.0280	19.4	880	2.0	0.010	0.018
	48	P2-7	2655.863	0.830	0.0291				0.018	0.011
	49	P2-6	2680.179	0.839	0.0274				0.013	0.014
	50	P2-5	2703.999	0.889	0.0184				0.009	0.009
	51	P2-4	2727.309	0.851	0.0252				0.013	0.012
	51	P2-8	2631.067	0.873	0.0212				0.010	0.011
3-12-79	1713	*P10-20	944.197	0.533	0.0983					
3-13-79	1717	P2-8	2631.067	0.829	0.0293	20.0	886	3.3	0.014	0.015
	19	P2-7	2655.863	0.778	0.0392				0.028	0.011
	21	P2-6	2680.179	0.809	0.0331				0.021	0.012
	23	P2-5	2703.999	0.867	0.0223				0.015	0.007
	25	P2-4	2727.309	0.846	0.0261				0.020	0.006
	27	P2-8	2631.067	0.864	0.0228				0.014	0.011
	28	P2-9	2605.806	0.842	0.0269				0.017	0.010
	30	P2-10	2580.096	0.666	0.0635				0.053	0.011
	31	P2-11	2553.952	0.856	0.0243				0.021	0.003
	33	P2-12	2527.391	0.864	0.0228				0.022	0.001
	35	P2-8	2631.067	0.914	0.0141				0.014	0.000
3-14-79	1618	P2-8	2631.067	0.822	0.0306	17.8	886	4.5	0.018	0.013
	20	P2-7	2655.863	0.742	0.0466				0.038	0.009
	21	P2-6	2680.179	0.783	0.0382				0.029	0.009
	22	P2-5	2703.999	0.816	0.0318				0.020	0.012
	24	P2-4	2727.309	0.778	0.0392				0.028	0.011
	26	P2-8	2631.067	0.803	0.0343				0.018	0.016
	30	P2-9	2605.806	0.805	0.0339				0.022	0.012
	32	P2-10	2580.096	0.649	0.0676				0.057	0.011

*CO_2 laser line

Continues

Table 1 — Laser Extinction Measurements and Calculated Molecular Absorption (continued)

Date	Local Time	Laser Line	ν (cm^{-1})	T	α (km^{-1})	Air Temp (°C)	Barometric Press. (mb)	ppH_2O (Torr)	CMA (km^{-1})	DIFF α−CMA (km^{-1})
3-14-79	1634	P2-11	2553.952	0.786	0.0376	17.8	886	4.5	0.025	0.013
	35	P2-12	2527.391	0.812	0.0325				0.024	0.012
	36	P2-8	2631.067	0.843	0.0267				0.018	0.009
3-15-79	1651	P2-8	2631.067	0.949	0.0082	20.0	880	5.0	0.019	-0.012
	53	P2-7	2655.863	0.824	0.0302				0.041	-0.011
	57	P2-6	2680.179	0.942	0.0093				0.031	-0.021
	58	P2-5	2703.999	0.944	0.0090				0.022	-0.013
	59	P2-4	2727.309	0.930	0.0113				0.030	-0.019
	1700	P2-8	2631.067	0.957	0.0069				0.019	-0.012
	02	P2-9	2605.806	0.898	0.0168				0.024	-0.007
	04	P2-10	2580.096	0.692	0.0575				0.057	0.005
	06	P2-11	2553.952	0.786	0.0376				0.025	0.013
	08	P2-12	2527.391	0.900	0.0165				0.025	-0.008
	10	P2-8	2631.067	0.940	0.0097				0.019	-0.009
3-16-79	1659	P2-8	2631.067	0.821	0.0308	21.7	878	4.0	0.016	0.015
	59	P2-7	2655.863	0.792	0.0364				0.032	0.002
	1700	P2-6	2680.179	0.819	0.0312				0.024	0.007
	02	P2-5	2703.999	0.851	0.0252				0.017	0.008
	03	P2-4	2727.309	0.823	0.0304				0.024	0.006
	05	P2-8	2631.067	0.849	0.0256				0.016	0.010
	07	P2-9	2605.806	0.839	0.0274				0.019	0.008
	09	P2-10	2580.096	0.629	0.0724				0.054	0.018
	10	P2-11	2553.952	0.795	0.0358				0.022	0.014
	13	P2-12	2527.391	0.809	0.0331				0.022	0.011
	14	P2-8	2631.067	0.865	0.0227				0.016	0.007
3-17-79	1645	P2-8	2631.067	0.762	0.0425	19.4	878	2.0	0.010	0.033
	46	P2-7	2655.863	0.725	0.0502				0.018	0.032
	47	P2-6	2680.179	0.769	0.0410				0.013	0.028
	48	P2-5	2703.999	0.784	0.0380				0.009	0.029
	49	P2-4	2727.309	0.768	0.0412				0.013	0.028
	52	P2-8	2631.067	0.776	0.0396				0.010	0.030
	54	P2-9	2605.806	0.753	0.0443				0.011	0.033
	55	P2-10	2580.096	0.575	0.0865				0.050	0.037
	57	P2-11	2553.952	0.748	0.0454				0.018	0.027
	59	P2-12	2527.391	0.763	0.0423				0.017	0.025
	1700	P2-8	2631.067	0.802	0.0345				0.010	0.025
3-18-79	1652	P2-8	2631.067	0.953	0.0075	15.6	879	2.5	0.012	-0.004
	54	P2-7	2655.863	0.0893	0.0177				0.022	-0.004
	55	P2-6	2680.179	0.934	0.0107				0.017	-0.008
	56	P2-5	2703.999	0.965	0.0056				0.012	-0.006
	59	P2-4	2727.309	0.944	0.0090				0.016	-0.007
	1702	P2-8	2631.067	0.954	0.0074				0.012	-0.005
	03	P2-9	2605.806	0.917	0.0135				0.014	-0.000
	05	P2-10	2580.096	0.688	0.0584				0.051	0.007
	06	P2-11	2553.952	0.870	0.0218				0.020	0.002
	08	P2-12	2527.391	0.880	0.0200				0.019	0.001
	09	P2-8	2631.067	0.962	0.0061				0.012	-0.006

Table 2 -- Summary of FTS and Laser Extinction Measurement Conditions

FTS Spectrum Iden.	Date	Local Time (MST)	FTS Config.	No. FTS Scans	FTS Meas. Path (km)	Laser Extinct. Meas. Time (MST)	Normalized FTS Spectrum
ASL01	3-14-79	1116	$InSb/CaF_2$	100	6.4	1630	
ASL02	3-14-79	1413	$InSb/CaF_2$	100	local	1630	
ASL03	3-14-79	1521	$InSb/CaF_2$	58	6.4	1630	
ASL04	3-14-79	1538	$InSb/CaF_2$	76	6.4	1630	ASL04RN
ASL05	3-14-79	1720	$InSb/CaF_2$	26	6.4	1630	
ASL06	3-14-79	1741	$InSb/CaF_2$	100	6.4	1630	ASL06RN
ASL07	3-15-79	1117	HgCdTe/KBr	100	local	1700	
ASL08	3-15-79	1510	HgCdTe/KBr	100	local	1700	
ASL09	3-15-79	1613	HgCdTe/KBr	91	6.4	1700	
ASL10	3-15-79	1740	HgCdTe/KBr	91	6.4	1700	
ASL11	3-16-79	1413	$InSb/CaF_2$	106	6.4	1705	
ASL13	3-16-79	1606	$InSb/CaF_2$	72	6.4	1705	ASL13RN
ASL14	3-16-79	1623	$InSb/CaF_2$	100	6.4	1705	ASL14RN
ASL15	3-16-79	1757	$InSb/CaF_2$	100	6.4	1705	ASL15RN
ASL16	3-17-79	1451	$InSb/CaF_2$	100	local	1652	
ASL17	3-17-79	1551	$InSb/CaF_2$	100	6.4	1652	ASL17RN
ASL18	3-17-79	1615	$InSb/CaF_2$	100	6.4	1652	ASL18RN
ASL19	3-17-79	1740	$InSb/CaF_2$	100	6.4	1652	ASL19RN
ASL20	3-17-79	1751	$InSb/CaF_2$	100	6.4	1652	ASL20RN
ASL21	3-18-79	1550	$InSb/CaF_2$	100	6.4	1700	
ASL22	3-18-79	1623	$InSb/CaF_2$	50	6.4	1700	ASL22RN
ASL23	3-18-79	1737	$InSb/CaF_2$	100	6.4	1700	ASL23RN
ASL24	3-20-79	1130	$InSb/CaF_2$	100	zero	none	ASL24R
ASL25	3-20-79	1203	$InSb/CaF_2$	100	zero	none	ASL25R
ASL26	3-21-79	1010	HgCdTe/KBr	100	zero	none	ASL26R
ASL27	3-21-79	1045	HgCdTe/KBr	100	zero	none	ASL27R
ASL28	3-21-79	1106	HgCdTe/KBr	100	zero	none	ASL28R

Table 3 — FTS Spectrum Normalization Parameters

Spectrum 1D				ASL04RN		ASL06RN	
Line 1D	ν (cm^{-1})	ν' (cm^{-1})	τ, Laser Trans.	τ', Spectrum Amplitude Adjacent Samples	δ ($\tau' - \tau$)	τ', Spectrum Amplitude Adjacent Samples	δ ($\tau' - \tau$)
P2-8	2631.067	2631.03	0.822	0.8305	+0.008	0.8229	+0.001
		2631.09		0.8293	+0.007	0.8271	+0.001
P2-7	2655.863	2655.86	0.742	0.7418	-0.002	0.7420	+0.000
P2-6	2680.179	2680.15	0.783	0.7799	-0.004	0.7772	-0.006
		2680.21		0.7751	-0.008	0.7715	-0.011
P2-5	2703.999	2703.95	0.816	0.8275	+0.009	0.8293	+0.013
		2704.01		0.8193	+0.003	0.8175	+0.002
P2-4	2727.309	2727.27	0.778	0.7866	+0.008	0.7924	+0.014
		2727.33		0.7944	+0.016	0.8062	+0.029
P2-8	2631.067	2631.03	0.803	0.8305	+0.027	0.8229	+0.020
		2631.09		0.8293	+0.026	0.8271	+0.024
P2-9	2605.806	2605.78	0.805	0.7883	-0.017	0.7892	-0.016
		2605.84		0.7764	-0.029	0.7817	-0.023
P2-10	2580.096	2580.05	0.649	0.5959	-0.054		
		2580.11		0.6932	+0.044		
P2-11	2553.952	2553.95	0.786	0.7822	-0.004	0.7801	-0.006
				0.7878	+0.001		
P2-12	2527.391	2527.38	0.812	0.7913	-0.021	0.7879	-0.015
		2527.44		0.7948	-0.018		
P2-8	2631.067	2631.03	0.843	0.8305	-0.014	0.8229	-0.020
		2631.09		0.8293	-0.013	0.8271	-0.016
Mean					-0.0010		+0.0007
Standard Deviation					±0.0225		±0.0159

Continues

Table 3 — FTS Spectrum Normalization Parameters (continued)

Spectrum 1D				ASL13RN		ASL14RN		ASL15RN	
Line 1D	ν (cm)	ν' (cm^{-1})	τ, Laser Trans.	τ', Spectrum Amplitude Adjacent Samples	δ ($\tau' - \tau$)	τ', Spectrum Amplitude Adjacent Samples	δ ($\tau' - \tau$)	τ', Spectrum Amplitude Adjacent Samples	δ ($\tau' - \tau$)
P2-8	2631.067	2631.03	0.821	0.8384	+0.019	0.8397	+0.019	0.8318	+0.011
		2631.09		0.8298	+0.008	0.8322	+0.011	0.8348	+0.014
P2-7	2655.863	2655.86	0.792	0.8227	+0.023	0.8226	+0.031	0.8258	+0.036
P2-6	2680.179	2680.15	0.819	0.7929	-0.016	0.8123	-0.007	0.8280	+0.009
		2680.21		0.7949	-0.024	0.8098	-0.009	0.8206	+0.002
P2-5	2703.999	2703.95	0.851	0.7985	-0.057	0.8110	-0.040	0.8320	-0.019
		2704.01		0.7960	-0.056	0.7987	-0.051	0.8249	-0.026
P2-4	2727.309	2727.27	0.823	0.8074	-0.016	0.7952	-0.028	0.8126	-0.010
		2727.33		0.7901	-0.033	0.7997	-0.023	0.8151	-0.008
P2-8	2631.067	2631.03	0.849	0.8384	-0.011	0.8397	-0.009	0.8318	-0.017
		2631.09		0.8298	-0.019	0.8322	-0.016	0.8348	-0.025
P2-9	2605.806	2605.78	0.839	0.8462	+0.007	0.8414	+0.002	0.8332	-0.006
		2605.84		0.8463	+0.007	0.8341	+0.005	0.8269	-0.012
P2-10	2580.096	2580.05	0.629						
		2580.11							
P2-11	2553.952	2553.95	0.795	0.8596	+0.065	0.8452	+0.050	0.8247	+0.029
P2-12	2527.391	2527.38	0.809	0.8524	+0.043	0.8378	+0.027	0.8142	+0.005
		2527.44		0.8506		0.8438	+0.035	0.8162	+0.007
P2-8	2631.067	2631.03	0.865	0.8384	-0.042	0.8397	-0.025	0.8318	-0.033
		2631.09		0.8298	-0.035	0.8322	-0.032	0.8348	-0.030
Mean					-0.0081		-0.0035		-0.0041
Standard Deviation					±0.0336		±0.0280		±0.0197

Continues

Table 3 — FTS Spectrum Normalization Parameters (continued)

Spectrum 1D				ASL17RN		ASL18RN	
Line 1D	ν (cm^{-1})	ν' (cm^{-1})	τ', Laser Trans.	τ', Spectrum Amplitude Adjacent Samples	δ ($\tau' - \tau$)	τ', Spectrum Amplitude Adjacent Samples	δ ($\tau' - \tau$)
P2-8	2631.067	2631.03	0.762	0.7867	+0.024	0.7809	0.019
		2631.09		0.7819	+0.020	0.7813	0.019
P2-7	2655.863	2655.86	0.725	0.7531	+0.022	0.7615	0.036
P2-6	2680.179	2680.15	0.769	0.7518	-0.017	0.7626	-0.006
		2680.21		0.7578	-0.011	0.7584	-0.011
P2-5	2703.999	2703.95	0.784	0.7610	-0.023	0.7751	-0.009
		2704.01		0.7507	-0.033	0.7703	-0.014
P2-4	2727.309	2727.27	0.768	0.7379	-0.030	0.7531	-0.015
		2727.33		0.7493	-0.019	0.7623	-0.006
P2-8	2631.067	2631.03	0.776	0.7867	+0.011	0.7809	0.005
		2631.09		0.7819	+0.006	0.7813	0.006
P2-9	2605.806	2605.78	0.753	0.7670	+0.014	0.7671	0.014
		2605.84		0.7697	+0.017	0.7624	0.009
P2-10	2580.096	2580.05	0.575			0.5713	-0.004
		2580.11				0.6879	0.109
P2-11	2553.952	2553.95	0.748	0.7593	+0.011	0.7531	0.005
P2-12	2527.391	2527.38	0.763	0.7695	+0.007	0.7582	-0.005
		2527.44		0.7665	+0.004	0.7565	-0.007
P2-8	2631.067	2631.03	0.802	0.7867	-0.015	0.7809	-0.019
		2631.09		0.7819	-0.020	0.7813	-0.019
Mean					-0.0018		0.0001
Standard Deviation					±0.0190		±0.0143

Continues

Table 3 — FTS Spectrum Normalization Parameters (continued)

Spectrum 1D				ASL19RN		ASL20RN	
Line 1D	ν (cm^{-1})	ν' (cm^{-1})	τ, Laser Trans.	τ', Spectrum Amplitude Adjacent Samples	δ ($\tau' - \tau$)	τ', Spectrum Amplitude Adjacent Samples	δ ($\tau' - \tau$)
P2-8	2631.067	2631.03	0.762	0.7828	0.021	0.7809	0.019
		2631.09		0.7867	0.025	0.7885	0.026
P2-7	2655.863	2655.86	0.725	0.7518	0.027	0.7488	0.024
P2-6	2680.179	2680.15	0.769	0.7616	-0.007	0.7565	-0.012
		2680.21		0.7549	-0.014	0.7437	-0.025
P2-5	2703.999	2703.95	0.784	0.7778	-0.006	0.7781	0.006
		2703.01		0.7763	-0.007	0.7653	-0.019
P2-4	2727.309	2727.27	0.768	0.7719	0.004	0.7535	-0.014
		2727.33		0.7725	0.004	0.7648	-0.003
P2-8	2631.067	2631.03	0.776	0.7828	0.007	0.7809	0.005
		2631.09		0.7867	0.011	0.7885	0.013
P2-9	2605.806	2605.78	0.753	0.7598	0.007	0.7614	0.008
		2605.84		0.7613	0.008	0.7567	0.004
P2-10	2580.096	2580.05	0.575	0.5660	-0.009	0.5748	0.000
		2580.11		0.6807	0.106	0.6888	0.113
P2-11	2553.952	2553.95	0.748	0.7417	-0.006	0.7531	0.005
P2-12	2527.391	2527.38	0.763	0.7442	-0.019	0.7529	-0.010
		2527.44		0.7465	-0.017	0.7570	-0.006
P2-8	2631.067	2631.03	0.802	0.7828	-0.019	0.7809	-0.021
		2631.09		0.7867	-0.013	0.7885	-0.016
Average					0.0003		-0.0016
Standard Deviation					±0.0147		±0.0155

Continues

Table 3 — FTS Spectrum Normalization Parameters (continued)

Spectrum 1D				ASL22RN		ASL23RN	
Line 1D	ν (cm^{-1})	ν' (cm^{-1})	τ, Laser Trans.	τ', Spectrum Amplitude Adjacent Samples	δ ($\tau' - \tau$)	τ', Spectrum Amplitude Adjacent Samples	δ ($\tau' - \tau$)
P2-8	2631.067	2631.03	0.953	0.9394	-0.013	0.9276	-0.025
		2631.09		0.9443	-0.009	0.9447	-0.008
P2-7	2655.863	2655.86	0.893	0.9199	0.037	0.9288	0.036
P2-6	2680.179	2680.15	0.934	0.9199	-0.014	0.8943	-0.040
		2680.21		0.9009	-0.034	0.9284	-0.006
P2-5	2703.999	2703.95	0.965	0.9480	-0.017	0.9193	-0.066
		2704.01		0.9386	-0.028	0.9128	-0.072
P2-4	2727.309	2727.27	0.944	0.9081	-0.036	0.8945	-0.050
		2727.33		0.9203	-0.024	0.9118	-0.032
P2-8	2631.067	2631.03	0.954	0.9394	-0.015	0.9276	-0.026
		2631.09		0.9443	-0.010	0.9447	-0.009
P2-9	2605.806	2605.78	0.917	0.9319	0.015	0.9324	0.015
		2605.84		0.9215	0.005	0.9476	0.031
P2-10	2580.096	2580.05	0.688	0.7032	0.015	0.5475	-0.140
		2580.11		0.9088	0.221	0.7988	0.111
P2-11	2553.952	2553.95	0.870	0.9239	0.054	0.9410	0.071
P2-12	2527.391	2527.38	0.880	0.9202	0.040	0.9458	0.066
		2527.44		0.9213	0.041	0.9144	0.034
P2-8	2631.067	2631.03	0.962	0.9394	-0.022	0.9276	-0.034
		2631.09		0.9443	-0.018	0.9447	-0.017
Average					0.0027		-0.0073
Standard Deviation					±0.0280		±0.0418

respectively, in Table 3. The next four columns list (a) the wavenumber of a spectrum sample, ν', (b) the measured laser transmission τ, (c) the individual amplitude τ' of a spectrum sample adjacent to or coincident with (to two decimal places) the appropriate laser line wavenumber, and (d) the difference δ between the amplitude of the spectrum sample and the actual transmission value measured at the laser frequency. The average of the δ values and standard deviation are listed at the bottom of each column of δ values. Values for τ' and δ for each of the spectra normalized by a given set of laser transmission values τ are repeated in successive columns in Table 3. As can be seen by examining the comparisons listed in the table, the average δ value or residual offset is typically a few tenths of a percent transmission. The random error in the normalization procedure approximated by the standard deviation in δ is generally less than ± 2% transmission except in cases where the spectral signal-to-noise ratio is poorer, e.g. spectra ASL13RN, ASL14RN, and ASL23RN. The measurement accuracy in an individual laser extinction measurement is estimated to be ± 3% under good measurement conditions. Nine or ten individual laser extinction measurements are averaged in arriving at the normalization factor used in scaling a given spectrum in units of absolute transmission. Thus, redundant laser transmission measurements should combine to produce an average scale factor accurate to about ± 1%. When applied to a given spectrum the resultant absolute transmission calibration should be valid to ± 2% in the best case of a high signal-to-noise ratio spectrum, with the accuracy correspondingly degraded to about ± 4 or 5% in cases where the spectrum signal-to-noise ratio is poorer.

Figures 4 thru 13 are graphic presentations of portions of two of the ratioed and normalized spectra listed in Table 1, namely ASL06RN and ASL17RN. These figures were reproduced from CRT displays of the spectra obtained with FTS system software. Reading from top to bottom of each column in each of the figures, the location of each of the laser line positions listed in Table 3 is shown. The top photograph shows the atmospheric transmission structure in the vicinity of the individual laser line which is specified at the bottom of each column. The lower photograph in each column shows the same portion of the spectrum at increased dispersion so that individual samples in the spectrum (0.06 cm^{-1} wide) are evident. The cursor in each photograph marks the spectrum location in cm^{-1} (top number) to two decimal places and the spectrum amplitude at that location to four decimal places. These values are the ν' and τ' values listed for spectra ASL06RN and ASL17RN in Table 3.

Some general observations can be made upon an examination of Figs. 4-13. The majority of the $2 \rightarrow 1$ band DF laser lines are located fortuitously at positions which are relatively free of coincidence with atmospheric absorption lines. The P2-10 located at 2580.096 cm^{-1} is the one notable exception (see Figs. 5 and 10). The P2-10 DF laser line is located on the shoulder of an N_2O absorption line. The periodic structure shown in the upper left-hand portion of Figs. 5 and 10 is a portion of the prominent N_2O absorption band located near 2565 cm^{-1}. Consequently, the P2-10 DF laser line is a poor choice for use in obtaining an absolute transmission normalization for the FTS spectra.

The substantial change in FTS spectrum amplitude values between the two adjacent spectrum samples for such a case as shown in Figs. 5 and 10 introduces a significant uncertainty into the laser transmission normalization procedure. Additional errors are introduced into the procedure due to any misregistration of the laser line position with the FTS spectrum. Both types of problems are minimized when laser line positions free from coincidence with absorption lines are used to derive the absolute transmission normalization.

Examples of the laser lines which are preferable for use in deriving the normalizations are the P2-8, P2-5, P2-4, and P2-12. The remaining DF laser lines, P2-7, P2-6, P2-9 and P2-11, can also be useful for derivation of absolute transmission normalization factors for the spectra obtained in these measurements. The data presented in this report were obtained under reduced total atmospheric pressure conditions at the WSMR elevation (875 mb at 1208 m above mean sea level (MSL)) and low atmospheric water vapor concentrations of 2-5 torr water vapor partial pressure; these parameters represent a more favorable case than would be obtained in general for long-path transmission spectra measured at sea level under higher water vapor partial pressure and/or higher total atmospheric pressure conditions. The P2-7, P2-6, P2-9, and P2-11 laser lines are sufficiently close to atmospheric HDO and H_2O absorption lines (P2-7, P2-6, and P2-9) and to an atmospheric N_2O absorption line (P2-11) so that appreciable overlap of the absorption line wing and the laser line position will occur under higher pressure conditions. This effect has been observed for comparisons similar to those shown in Figs. 4-13 for sea-level spectra taken at San Nicolas Island, California, over a 4-km path during absolute humidity conditions averaging around 10 g/m^3 H_2O. For the comparisons listed in Table 3 and shown in Figures 4-13, the amplitude of a spectrum sample value (τ' values listed in Table 3) varies usually no more than 1% in absolute transmission between two adjacent samples which bracket the position of the $2 \rightarrow 1$ band DF laser line used to normalize the spectrum for absolute transmission. The notable exception is the P2-10 line as previously observed. Accordingly, the average multiplicative normalization factor derived by comparing measured laser transmission to spectrum sample amplitudes at each of the ν' values shown in Table 3 did not include the measurements for the P2-10 line. For higher total pressure and higher water vapor conditions, omission of data for additional laser lines would be appropriate as discussed above.

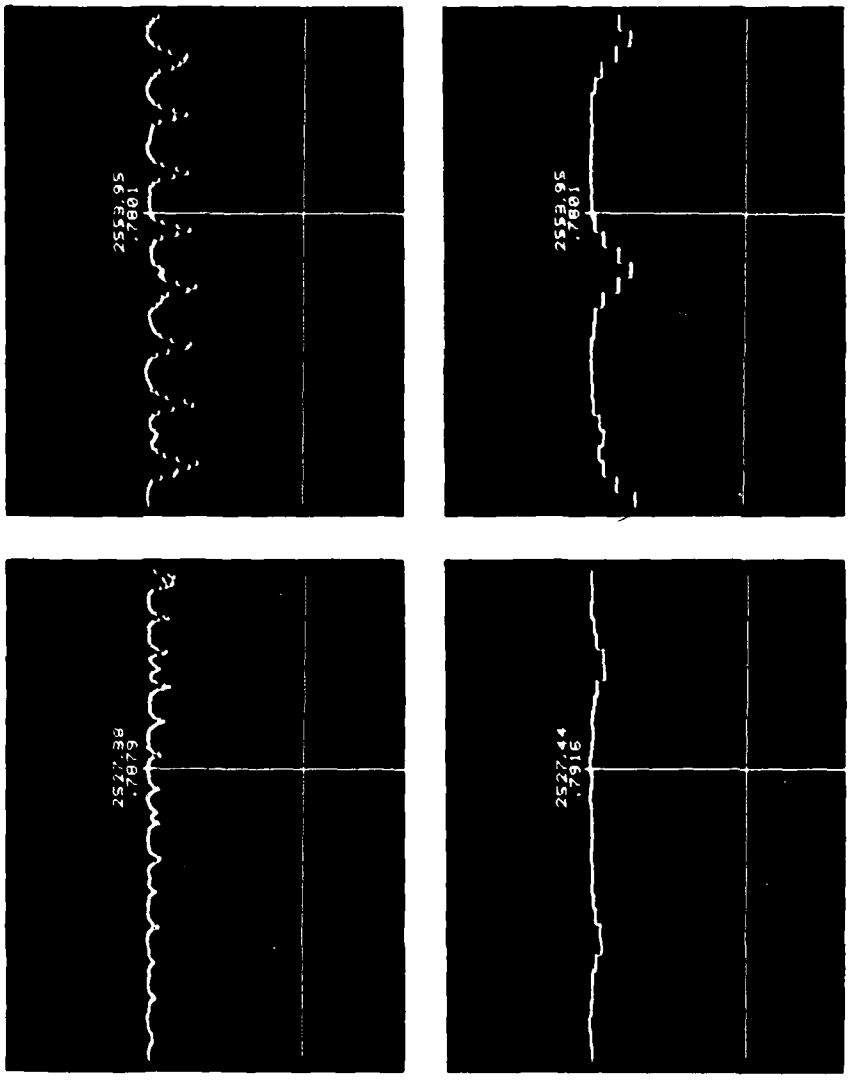

Fig. 4 — Oscilloscope trace showing normalized spectrum structure and absolute transmission amplitude in the vicinity of DF laser lines: Spectrum ASL06RN, P2-12 (left) and P2-11 (right)

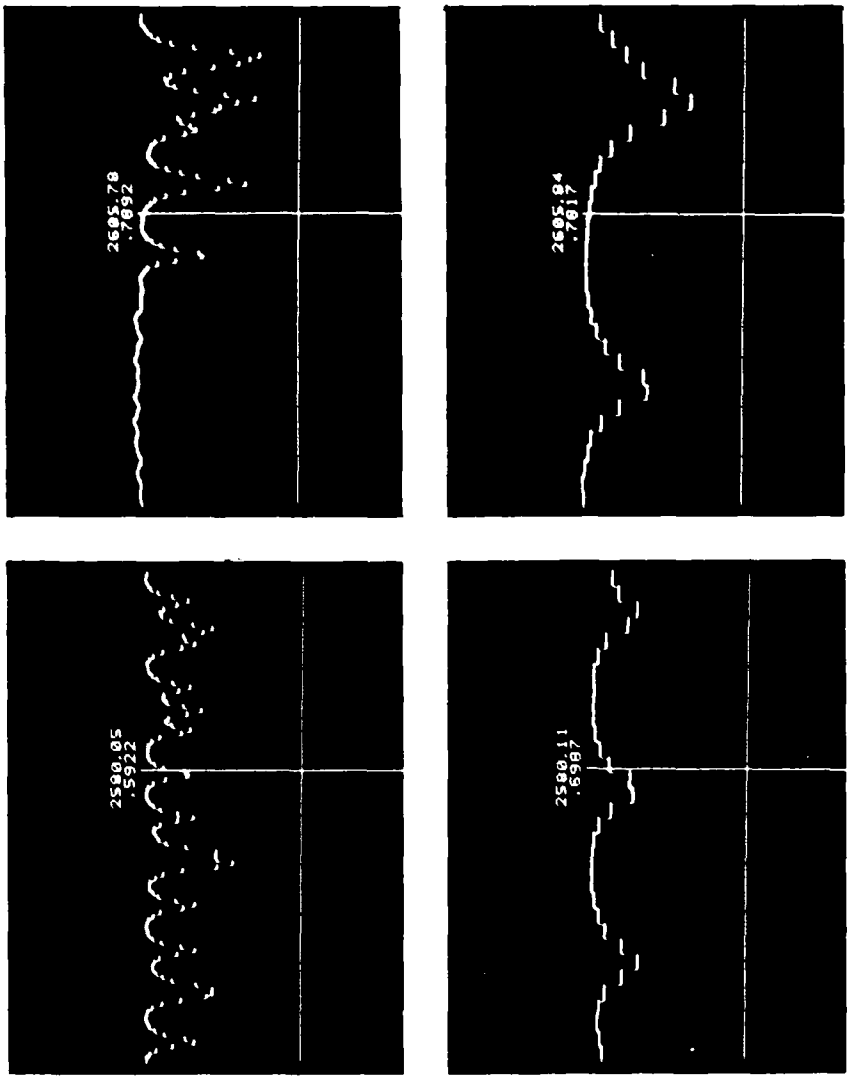

Fig. 5 — Oscilloscope trace showing normalized spectrum structure and absolute transmission amplitude in the vicinity of DF laser lines: spectrum ASL06RN, P2-10 (left) and P2-9 (right)

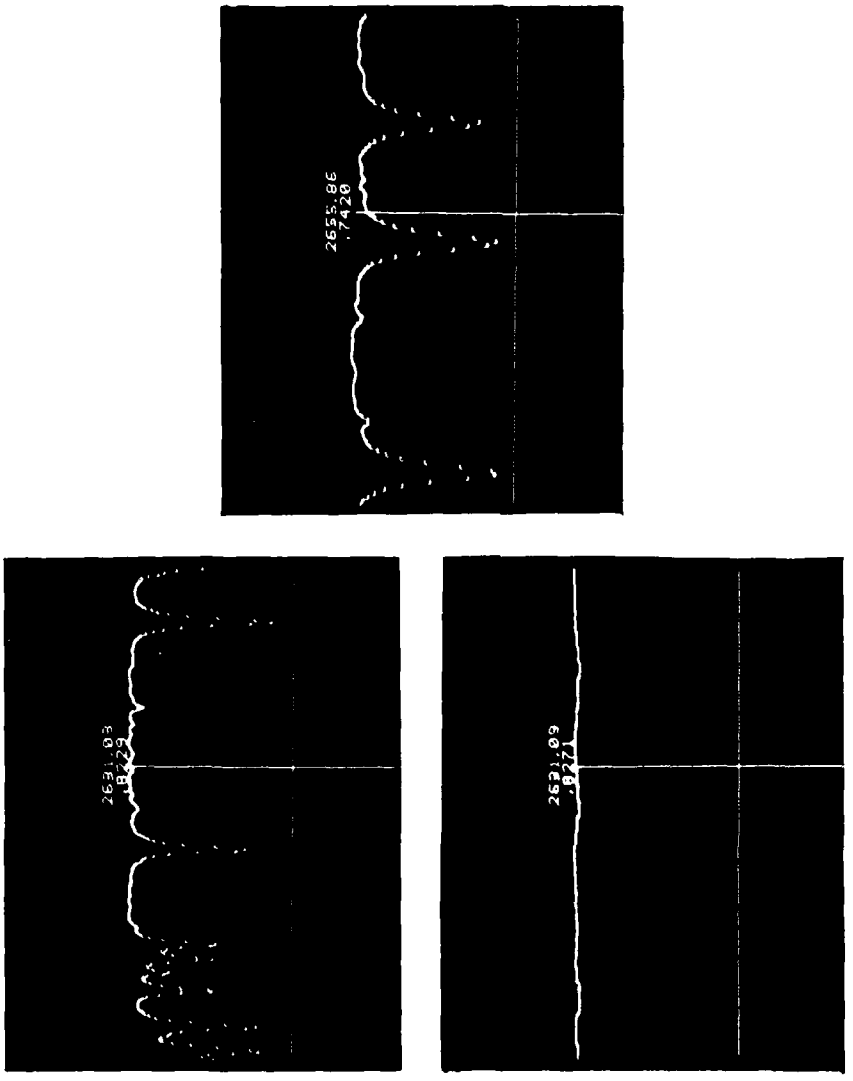

Fig. 6 — Oscilloscope trace showing normalized spectrum structure and absolute transmission amplitude in the vicinity of DF laser lines: spectrum ASL06RN, P2-8 (left) and P2-7 (right)

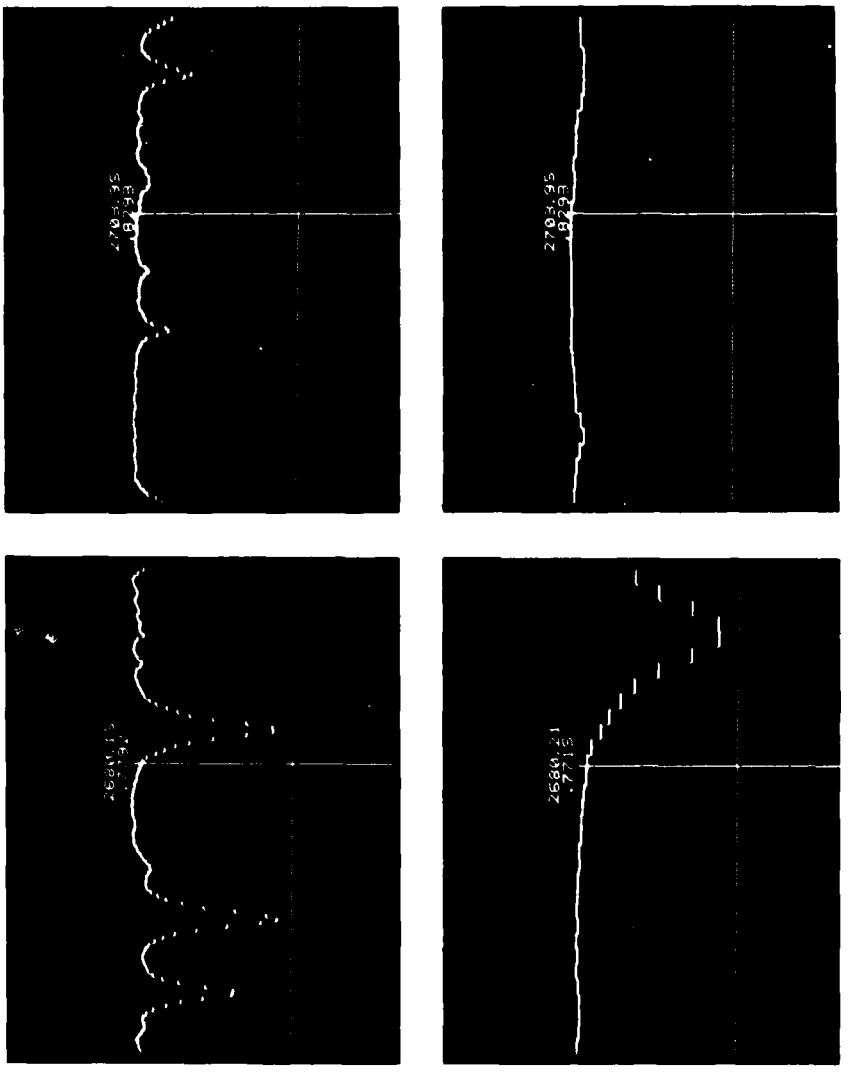

Fig. 7 — Oscilloscope trace showing normalized spectrum structure and absolute transmission amplitude in the vicinity of the DF laser lines: spectrum ASL06RN, P2-6 (left) and P2-5 (right)

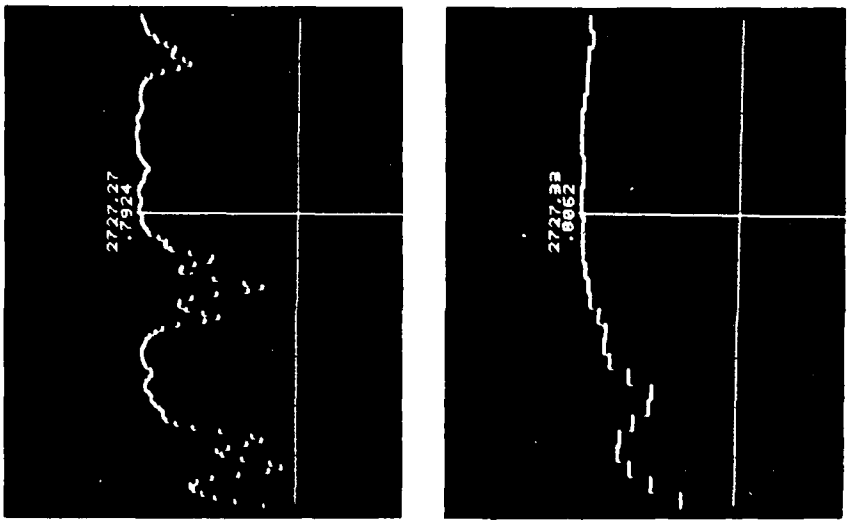

Fig. 8 — Oscilloscope trace showing normalized spectrum structure and absolute transmission amplitude in the vicinity of DF laser lines: spectrum ASL06RN, P2-4

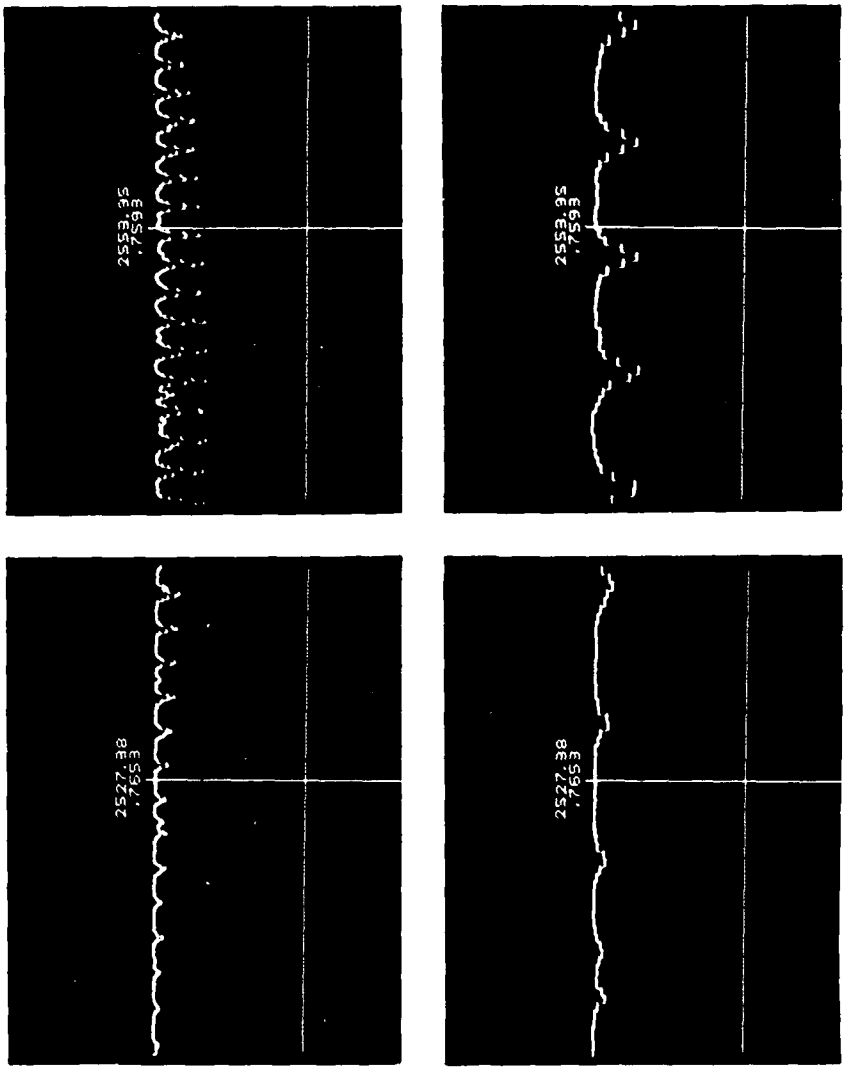

Fig. 9 — Oscilloscope trace showing normalized spectrum structure and absolute transmission amplitude in the vicinity of DF laser lines: spectrum ASL17RN, P2-12 (left) and P2-11 (right

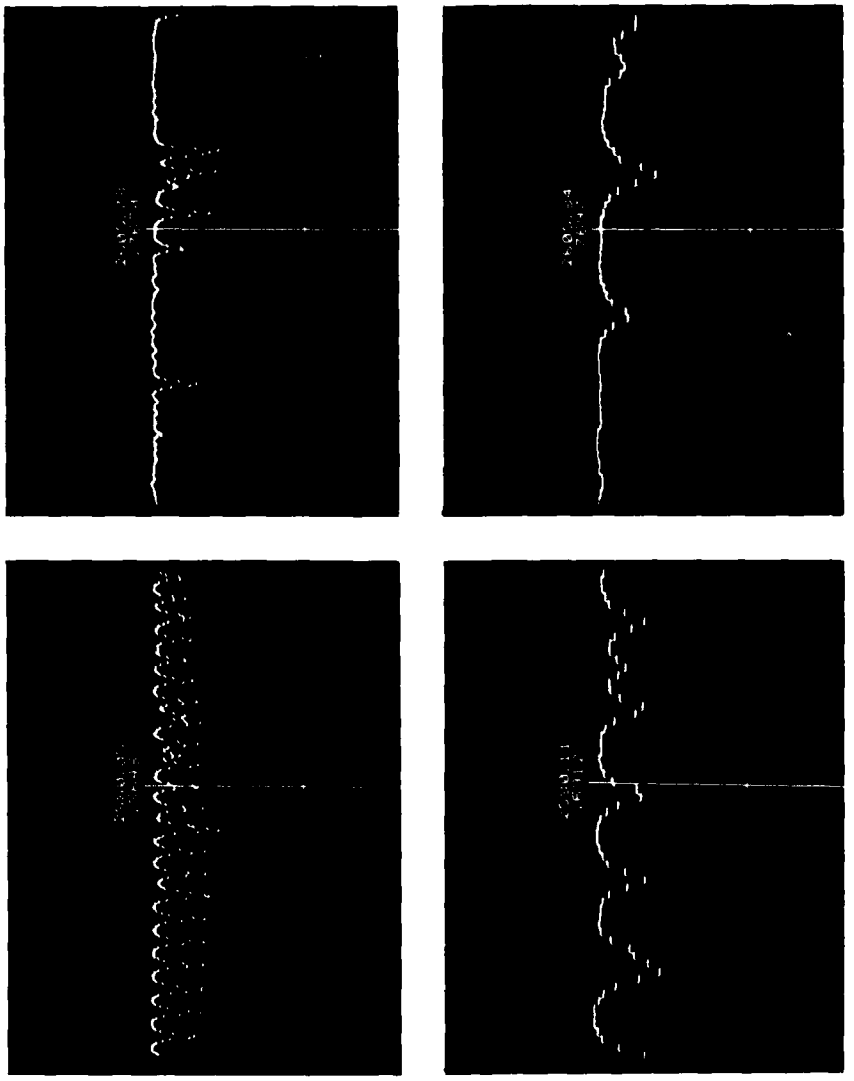

Fig. 10 — Oscilloscope trace showing normalized spectrum structure and absolute transmission amplitude in the vicinity of DF laser lines: spectrum ASL17RN, P2-10 (left) and P2-9 (right)

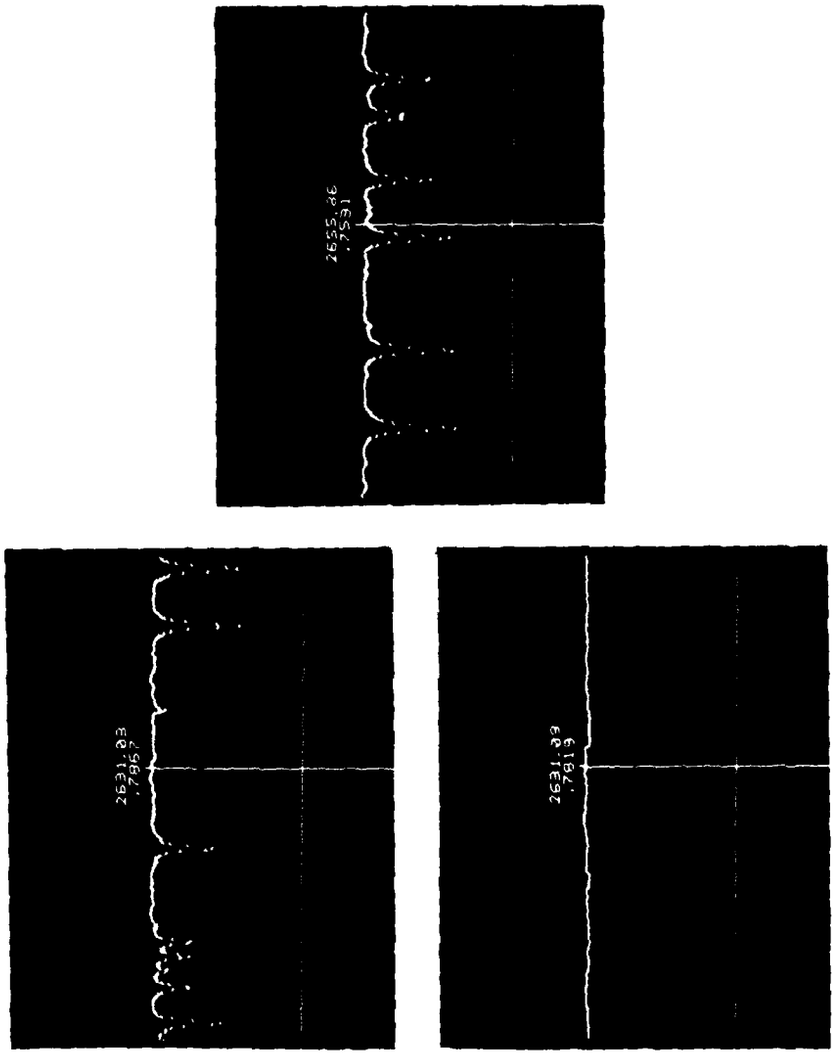

Fig. 11 — Oscilloscope trace showing normalized spectrum structure and absolute transmission amplitude in the vicinity of DF laser lines: spectrum ASL17RN, P2-8 (left) and P2-7 (right)

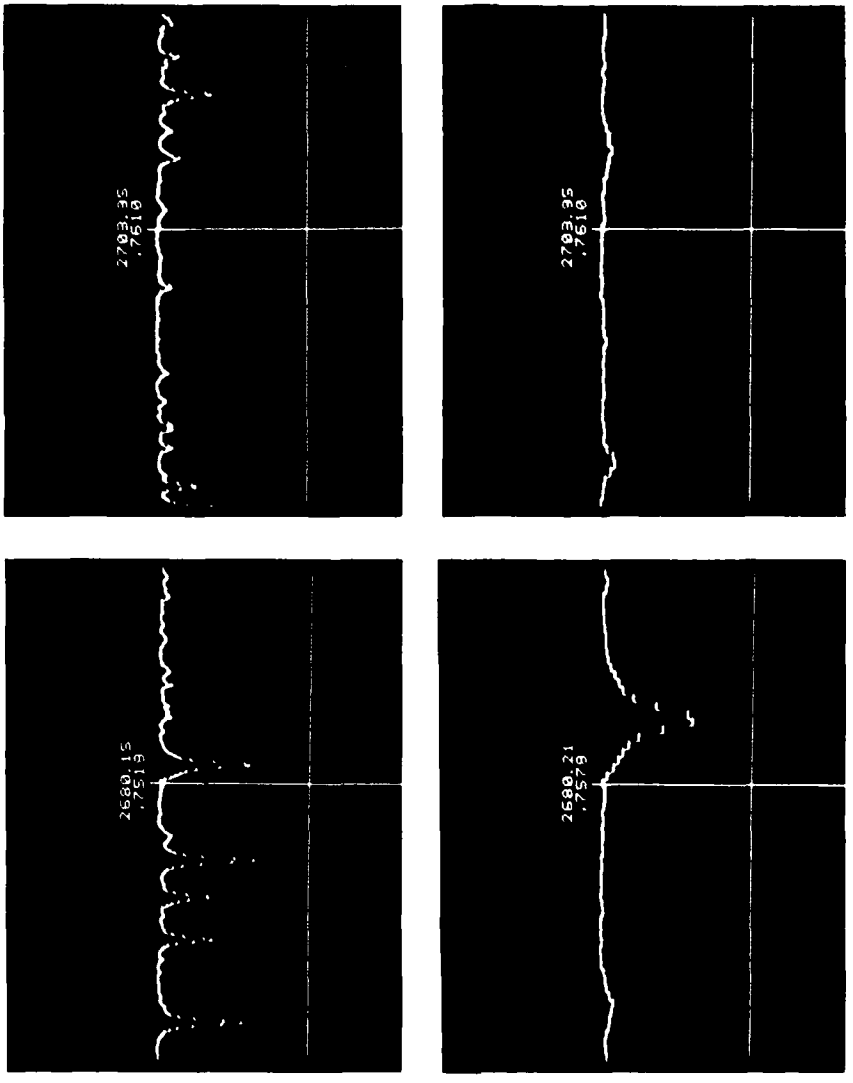

Fig. 12 — Oscilloscope trace showing normalized spectrum structure and absolute transmission amplitude in the vicinity of DF laser lines: spectrum ASL17RN, P2-6 (left) and P2-5 (right)

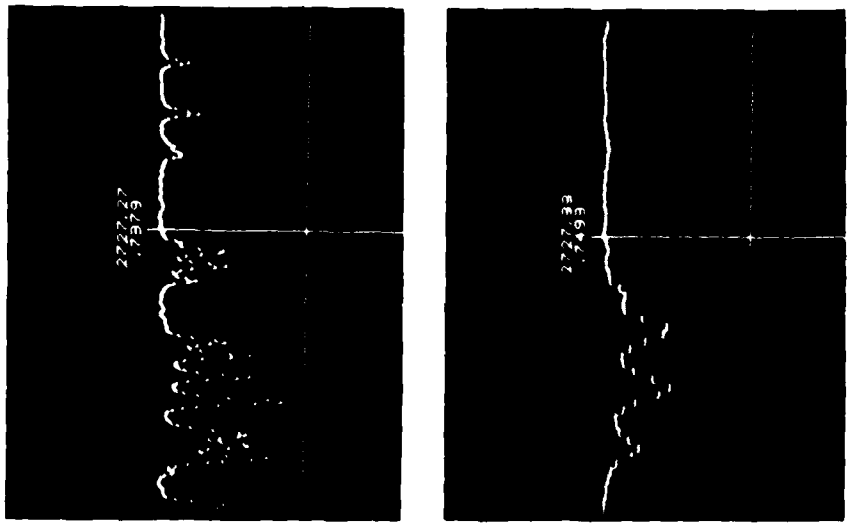

Fig. 13 — Oscilloscope trace showing normalized spectrum structure and absolute transmission amplitude in the vicinity of DF laser lines: spectrum ASL17RN, P2-4

3.2.2 Path-Integrated Molecular Absorber Concentrations

Figures 14 and 15 are plots of limited portions of three of the ratioed, normalized spectra listed in Table 2, for the spectral interval 2680-2800 cm^{-1}. Several reasonably well isolated HDO absorption lines appear in this region, and absorption profiles of these lines provide a measure of path-integrated average concentrations of this isotope occurring during the measurement times. Using the standard sea-level model atmospheric abundance ratio of 0.03% HDO/H_2O [5], the path-integral HDO measurements can be used to infer path-integral values for water vapor concentrations along the path. In the 2680- to 2800-cm^{-1} region shown, only a few relatively weak H_2O absorption lines can be identified, in contrast to the typical condition of very strong H_2O absorption lines in most regions of the near infrared. Provided that the accepted value for the sea-level HDO/H_2O ratio is correct, the spectral regions of the aforementioned figures are then quite useful for determining average absolute humidities over long atmospheric paths.

In addition to the few weak H_2O absorption lines which can be identified in the spectral regions shown in Figs. 14 and 15, a few weak, relatively isolated absorption lines of methane and nitrous oxide can also be identified.

Table 4 contains a list of the spectral features identified for the three spectra shown in Figs. 14 and 15. Column 1 of the table lists the line position contained in the 1978 edition of the AFGL line atlas [6]. The second column contains the observed line position measured from the spectral records shown in Figures 14 and 15, generally to a precision of 0.05 cm^{-1}. Columns 3, 4, and 5 contain the species identification, line strength, and line half-width, respectively, as contained in Ref. 10. The same notation for molecular species used in Ref. 5 is used, namely 162 = HDO, 161 = H_2O, 211 = CH_4, and 446 = N_2O. The last column of Table 4 lists the transmission at line center (maximum absorption) for each of the prominent absorption lines identified in spectrum ASL04RN. The AFGL line atlas [5,6] lists over 2600 lines in the 2680- to 2800-cm^{-1} region, whereas Table 4 contains an identification of 165 these for which the product of line strength and concentration is highest. The observed line positions (Column 2 of Table 4) are consistently about 0.05-0.07 cm^{-1} less than the AFGL values listed in Column 1, which is the limiting accuracy of the FTS hardware and plotting software. Improvements in the FTS frequency scale calibration to < 0.05 cm^{-1} are possible by using independent measurements of multiline laser spectra and interpolation procedures; this was not done for the spectra shown in Figs. 14 and 15 which are sufficiently well calibrated in frequency to provide unambiguous comparisons to the spectral lines listed in Column 1 of Table 4.

Path-integral molecular absorber concentrations were derived by simply measuring the peak absorption (minimum transmission) values of each absorption line at line center and relating this measurement (corrected for the spectral line base absorption value, i.e. local transmission maximum) to the average numerical density of a particular molecule along the absorption path. This procedure is less exact than integrating the area under a spectral absorption line and equating that value to the line strength, particularly when the line profile suffers significant modification due to the effects of finite resolution of the measuring instrument. In the present case the full base width of the unapodized FTS instrument function is 0.0625 cm^{-1} or about 0.05 cm^{-1} for an apodized spectrum using a conventional spectroscopic definition (Rayleigh criterion).

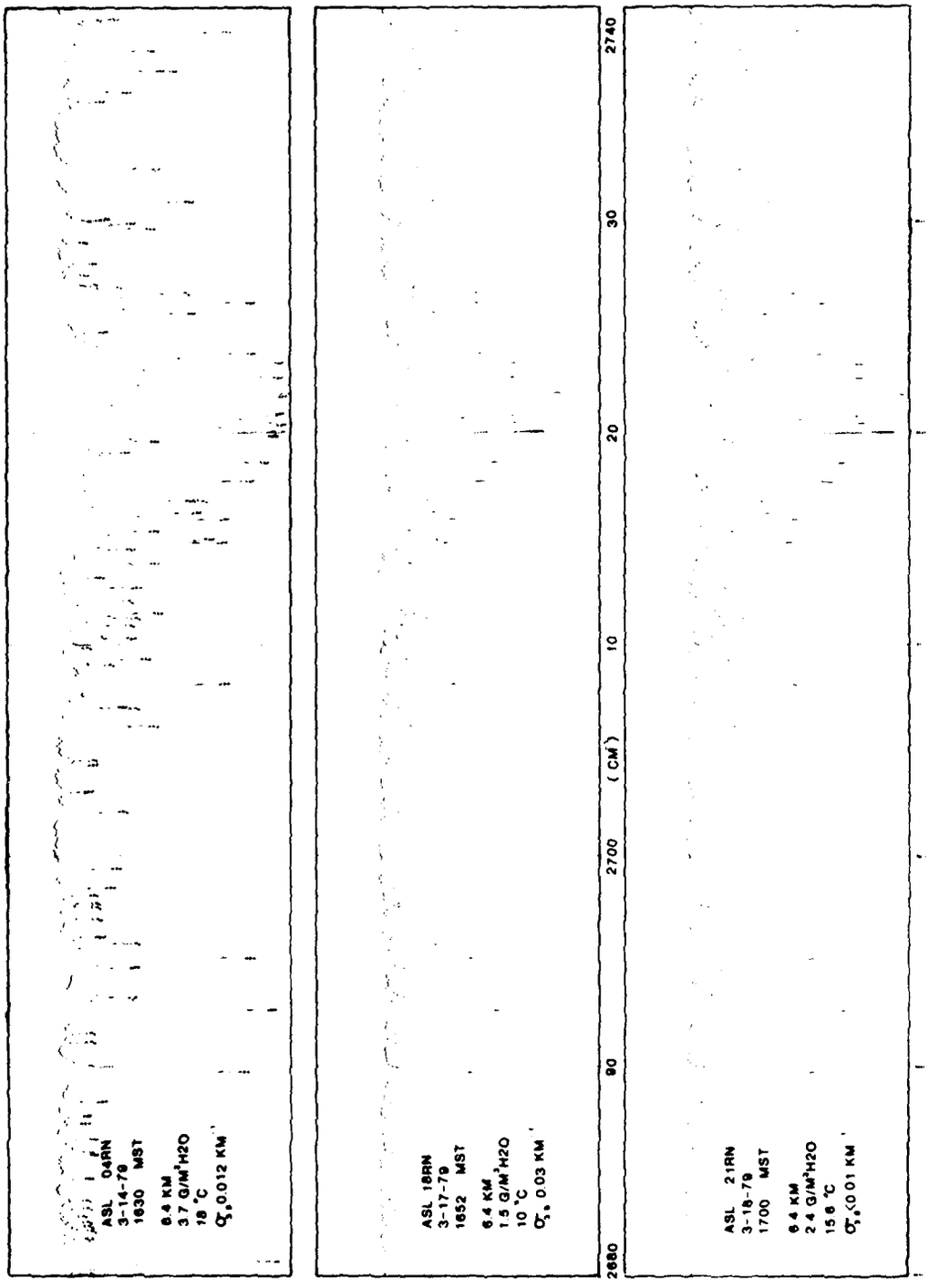

Fig. 14 — Spectra ASL04RN, ASL18RN, and ASL21RN, 2680 cm^{-1} to 2740 cm^{-1}

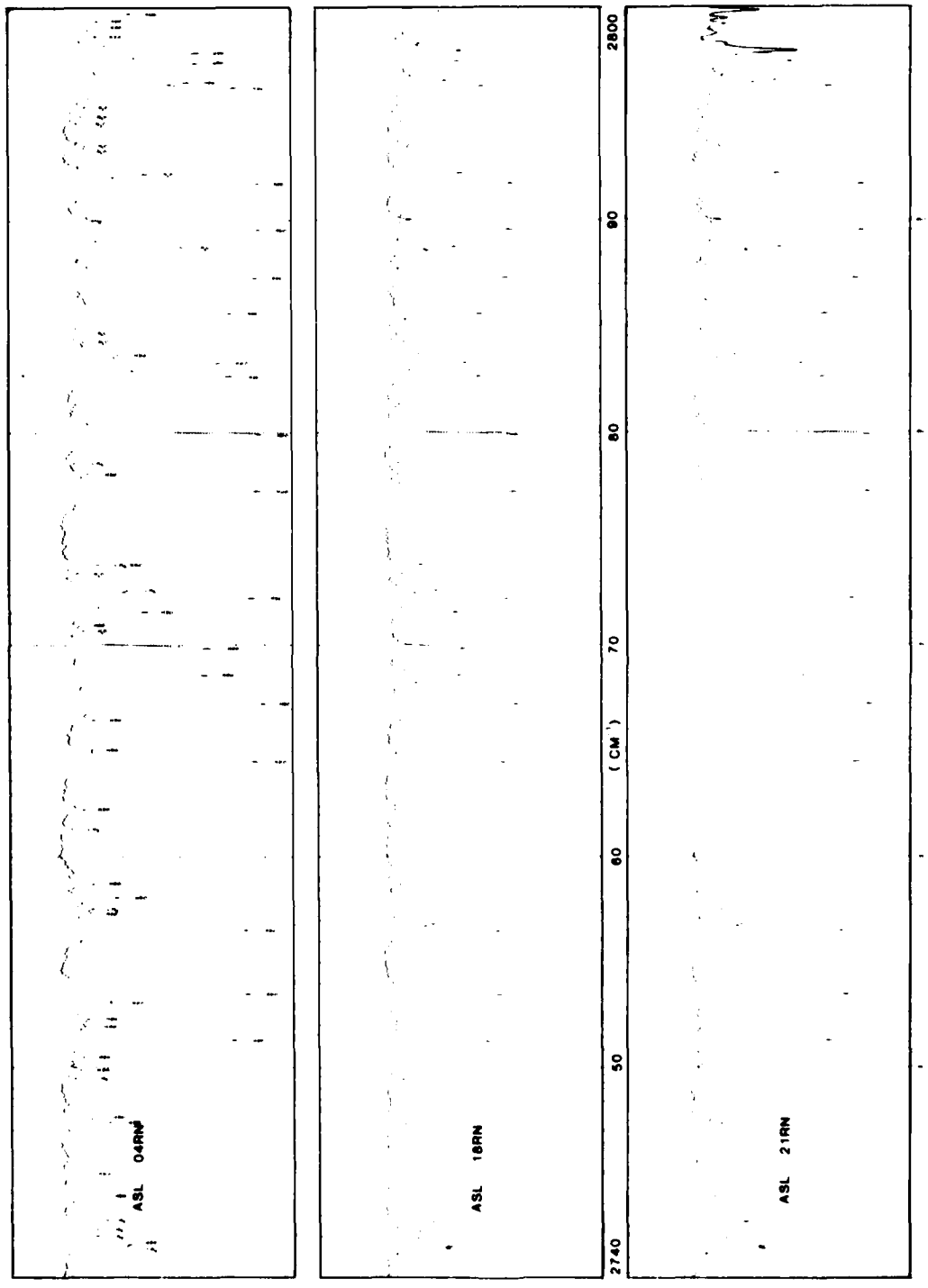

Fig. 15 — Spectra ASL04RN, ASL18RN, and ASL21RN, 2740 cm^{-1} to 2800 cm^{-1}

Table 4 — FTS Spectral Line Identifications and Measured Transmissions (ASL04RN)

Line Pos. Calculated	Line Pos. Observed	Species*	S (cm^{-1}/molecule cm^{-2})	α (cm^{-1})	T
2680.759	2680.70	162	0.776 E-23	0.096	0.103
2681.792	2681.75	161	0.149 E-24	0.046	0.770
2682.230	2682.20	211	0.316 E-21	0.055	0.757
2682.420	2682.35	211	0.228 E-21	0.055	0.775
2682.610	2682.55	211	0.246 E-21	0.055	0.790
2682.860	2682.80	211	0.702 E-22	0.055	0.807
2683.250	2683.20	211	0.263 E-21	0.055	0.772
2683.640	2683.60	211	0.281 E-21	0.055	0.775
2684.686	2684.65	162	0.153 E-24	0.086	0.770
2685.970	2685.90	162	0.303 E-24	0.087	0.728
2682.562	2686.50	162	0.333 E-24	0.089	0.758
2687.267	2687.20	162	0.113 E-24	0.096	0.792
2687.646	2687.55	162	0.130 E-24	0.096	0.782
2688.372	2688.30	162	0.300 E-24	0.084	0.737
2689.785	2689.75	162	0.511 E-23	0.107	0.232
2691.200	2691.15	211	0.281 E-21	0.055	0.772
2691.590	2691.50	211	0.263 E-21	0.055	0.768
2692.750	2692.70	162	0.739 E-23	0.103	0.130
2693.335	2693.30	161	0.425 E-24	0.061	0.624
2694.708	2694.65	162	0.905 E-24	0.094	0.624
2695.208	2695.15	162	0.522 E-23	0.098	0.221
2695.820 B†					
2696.010 B†	2695.85	211	0.694 E-21	0.054	0.610
2696.203	2696.15	162	0.167 E-24	0.086	0.735
2697.000 B†					
2697.120 B†	2697.05	211	0.351 E-21	0.055	0.750
2697.650	2697.60	211	0.350 E-21	0.054	0.756
2697.810	2697.75	211	0.386 E-21	0.055	0.745
2698.168	2698.10	162	0.153 E-24	0.098	0.766
2698.528	2698.45	162	0.417 E-24	0.093	0.702
2699.420	2699.35	162	0.682 E-24	0.091	0.688
2702.119	2702.10	162	0.215 E-24	0.094	0.660
2703.093	2703.05	162	0.262 E-24	0.086	0.770
2704.458	2704.40	162	0.198 E-24		
2704.560	2704.50	211	0.246 E-21	0.055	0.758
2706.216	2706.15	162	0.153 E-23	0.097	0.557
2707.150	2707.05	211	0.175 E-22	0.055	0.655
2708.179	2708.15	162	0.417 E-23	0.099	0.300
2709.050	2709.05	211	0.228 E-21	0.055	0.708
2709.340	2709.25	162	0.135 E-23	0.094	0.585
2710.080	2710.00	211	0.175 E-22	0.055	0.745
2710.336	2710.30	162	0.344 E-24	0.044	0.640
2710.960	2710.90	211	0.175 E-21	0.055	0.638
2711.260	2711.25	211	0.422 E-21	0.055	0.608

*161 = H_2O, 162 = HDO, 211 = CH_4, 446 = N_2O.

Continues

†B denotes unresolved blend.

Table 4 — FTS Spectral Line Identifications and Measured Transmissions (*ASL04RN*) (*continued*)

Line Pos. Calculated	Line Pos. Observed	Species*	S (cm^{-1}/molecule cm^{-2})	α (cm^{-1})	T
2711.270	2711.50	211	0.333 E-21	0.055	0.528
2711.515	2711.50	162	0.258 E-24	0.061	0.529
2712.060	2712.05	211	0.515 E-21	0.055	0.639
2712.741	2712.70	162	0.708 E-27	0.037	0.606
2713.212	2713.15	162	0.307 E-24	0.075	0.740
2713.866	2713.80	162	0.540 E-24	0.056	0.546
2713.879	2713.80	162	0.540 E-24	0.056	0.546
2714.535	2714.50	162	0.654 E-24	0.071	0.728
2714.853	2714.82	162	0.139 E-23	0.031	0.312
2714.966	2714.92	162	0.270 E-23	0.098	0.355
2715.407	2715.35	162	0.118 E-23	0.085	0.532
2715.958	2715.90	162	0.106 E-23	0.047	0.295
2716.271	2716.20	162	0.255 E-23	0.094	0.390
2716.810	2716.80	162	0.130 E-23	0.070	0.315
2716.840	2716.80	211	0.702 E-22	0.055	0.315
2716.913	2716.80	162	0.130 E-23	0.070	0.315
2716.933	2716.80	162	0.353 E-25	0.081	0.315
2717.751	2717.70	162	0.398 E-23	0.040	0.195
2718.647	2718.60	162	0.245 E-23	0.063	0.145
2718.682	2718.60	162	0.245 E-23	0.063	0.145
2719.007	2719.05	162	0.322 E-25	0.083	0.655
2719.116	2719.05	162	0.322 E-25	0.086	0.655
2719.631	2719.60	162	0.117 E-23	0.085	0.532
2720.132	2720.05	162	0.442 E-23	0.055	0.048
2720.136	2720.05	162	0.442 E-23	0.055	0.048
2720.495	2720.50	162	0.464 E-23	0.095	0.063
2720.553	2720.50	162	0.414 E-23	0.082	0.063
2720.838	2720.80	162	0.562 E-23	0.102	0.075
2720.900	2720.80	162	0.285 E-25	0.093	0.075
2721.877	2721.85	162	0.733 E-23	0.077	0.025
2721.934	2721.85	162	0.733 E-23	0.077	0.025
2722.664	2722.60	162	0.848 E-23	0.096	0.092
2723.338	2723.30	162	0.847 E-23	0.096	0.079
2723.777	2723.75	162	0.461 E-23	0.095	0.200
2724.798	2724.75	162	0.121 E-24	0.094	0.719
2725.682	2725.65	162	0.249 E-23	0.094	0.408
2726.161	2726.10	162	0.558 E-23	0.102	0.207
2726.630	2726.60	211	0.874 E-21	0.057	0.440
2727.528	2725.50	162	0.104 E-24		
2728.060	2728.00	162	0.253 E-24	0.100	0.757
2729.007	2728.95	162	0.105 E-24	0.086	0.790
2729.010	2728.95	162	0.357 E-25	0.096	0.790
2729.675	2729.65	162	0.129 E-23	0.094	0.555

*161 = H_2O, 162 = HDO, 211 = CH_4, 446 = N_2O

Continues

Table 4 -- FTS Spectral Line Identifications and Measured Transmissions (ASL04RN) (continued)

Line Pos. Calculated	Line Pos. Observed	Species*	S (cm^{-1}/molecule cm^{-2})	α (cm^{-1})	T
2729.900	2729.80	162	0.559 E-24	0.095	0.620
2730.928	2730.88	162	0.265 E-23	0.098	0.415
2732.491	2732.45	161	0.107 E-23	0.058	0.535
2735.682	2735.65	162	0.295 E-24	0.095	0.738
2736.108	2736.05	162	0.632 E-24	0.091	0.636
2737.121	2737.10	162	0.609 E-24	0.101	0.518
2737.096	2737.10	162	0.485 E-24	0.099	0.518
2738.052	2738.05	162	0.148 E-23	0.097	0.540
2738.923	2738.90	162	0.419 E-23	0.099	0.285
2739.555	2739.50	446	0.770 E-23	0.075	0.720
2739.489	2739.50	162	0.224 E-24	0.100	0.720
2741.478	2741.45	211	0.960 E-21	0.059	0.589
2741.602	2741.55	162	0.998 E-21	0.051	0.572
2741.993	2741.90	211	0.556 E-21	0.059	0.688
2742.314	2742.25	211	0.564 E-21	0.059	0.688
2742.755	2742.70	211	0.872 E-21	0.051	0.652
2743.941	2743.85	162	0.526 E-24	0.096	0.685
2744.965	2744.90	162	0.297 E-24	0.089	0.750
2747.412	2747.35	162	0.851 E-24	0.094	0.645
2747.623	2747.55	162	0.194 E-24	0.097	0.712
2749.490	2749.45	211	0.404 E-21	0.055	0.766
2749.920	2749.85	162	0.239 E-24	0.095	0.750
2750.503	2750.45	162	0.220 E-24	0.094	0.740
2751.342	2751.25	162	0.529 E-23	0.098	0.198
2752.007	2751.95	162	0.199 E-24	0.093	0.733
2752.339	2752.25	162	0.226 E-24	0.096	0.721
2753.112	2753.05	162	0.351 E-24	0.102	0.642
2753.545	2753.50	162	0.746 E-23	0.103	0.149
2756.558	2756.50	162	0.512 E-23	0.102	0.160
2757.377	2757.35	162	0.313 E-24	0.098	0.713
2757.600	2757.55	211	0.449 E-21	0.061	0.703
2758.092	2758.08	162	0.366 E-24	0.098	0.612
2758.751	2758.70	162	0.492 E-24	0.092	0.702
2761.350	2761.30	211	0.421 E-21	0.055	0.779
2762.267	2762.20	162	0.331 E-24	0.102	0.734
2764.551	2764.50	162	0.793 E-23	0.096	0.120
2765.119	2765.05	162	0.257 E-24	0.103	0.705
2766.506	2766.45	162	0.301 E-24	0.099	0.696
2767.277	2767.20	162	0.925 E-23	0.101	0.095
2768.634	2768.60	162	0.381 E-23	0.095	0.295
2769.897	2769.85	162	0.378 E-23	0.096	0.290
2770.717	2770.65	161	0.122 E-24	0.073	0.735
2770.908	2770.90	162	0.886 E-25	0.096	0.751

*161 = H_2O, 162 = HDO, 211 = CH_4, 446 = N_2O

Continues

Table 4 — FTS Spectral Line Identifications and Measured Transmissions (ASL04RN) (continued)

Line Pos. Calculated	Line Pos. Observed	Species*	S (cm^{-1}/molecule cm^{-2})	α (cm^{-1})	T
2771.614	2771.60	162	0.282 E-24	0.090	0.507
2722.259	2722.20	162	0.739 E-23	0.099	0.131
2722.630	2772.60	211	0.404 E-21	0.055	
2722.657	2722.60	211	0.524 E-21	0.055	
2773.404	2773.40	446	0.454 E-21	0.077	0.752
2773.872	2773.80	211	0.607 E-21	0.063	0.680
2777.301	2777.25	162	0.878 E-23	0.095	0.110
2778.148	2778.10	162	0.197 E-24	0.098	0.720
2778.640	2778.60	211	0.263 E-21	0.055	0.765
2779.969	2779.90	162	0.953 E-23	0.098	0.105
2782.718	2782.70	162	0.526 E-23	0.093	0.207
2783.353	2783.30	162	0.210 E-23	0.081	0.244
2783.722	2783.70	162	0.418 E-24	0.102	0.620
2784.351	2784.30	446	0.153 E-22	0.093	0.732
2784.355	2784.30	446	0.153 E-22	0.110	0.732
2784.748	2784.70	446	0.499 E-23	0.082	0.733
2784.742	2784.70	446	0.499 E-23	0.082	0.733
2785.659	2785.60	162	0.515 E-23	0.095	0.208
2787.333	2787.30	162	0.773 E-23	0.096	0.120
2788.811	2788.75	161	0.121 E-23	0.076	0.377
2789.593	2789.55	162	0.828 E-23	0.094	0.108
2791.759	2791.70	162	0.866 E-23	0.096	0.112
2792.253	2792.20	446	0.555 E-22	0.070	0.503
2793.411	2793.40	446	0.130 E-21	0.073	0.730
2793.628	2793.50	446	0.152 E-21	0.073	0.725
2793.840	2793.75	446	0.177 E-21	0.074	0.750
2794.638 } B†	2794.60	446	0.309 E-21	0.075	0.752
2794.702 }	2794.60	446	0.548 E-22	0.086	
2795.008	2794.95	446	0.398 E-21	0.075	0.737
2795.431	2795.40	162	0.206 E-24	0.098	0.726
2796.294	2796.25	162	0.525 E-23	0.092	0.186
2796.577	2796.50	162	0.911 E-24	0.065	0.355
2797.472	2797.40	162	0.272 E-23	0.081	0.328
2797.971	2797.90	162	0.271 E-23	0.084	0.322
2798.747	2798.70	162	0.313 E-24	0.095	0.682
2799.189	2799.15	162	0.126 E-25	0.089	0.673
2799.193	2799.15	162	0.873 E-25	0.083	0.673
	2799.45				
2799.787	2799.75	162	0.576 E-24	0.096	0.564

*161 = H_2O, 162 = HDO, 211 = CH_4, 446 = N_2O.

†B denotes unresolved blend.

This value is 25-50% of the half width of most of the lines listed in Table 4 and accordingly does not contribute significantly to a reduction in peak line intensity. HITRAN calculations were performed for conditions corresponding to the measurements shown in Figs. 14 and 15, including convolution with $(\sin x)/x$ instrument functions. Very minor differences are apparent between infinite resolution calculations and those done with instrument functions up to 0.08 cm^{-1}; therefore it was determined that the errors introduced by measuring peak absorption line transmission as opposed to integrated line area would be less than 10%. A more important factor contributing to errors in determining path-integral molecular concentrations from the spectra shown in Figs. 14 and 15 for many cases is the blending of many weak unresolved lines with a marginally stronger line being measured. This situation exists for most of the H_2O, CH_4, and N_2O lines measured here. Only a rigorous correction for the contribution of the several weaker blending lines would improve the measurement accuracy for these weaker lines. Such an analysis procedure can only be realistically accomplished using several iterations with a HITRAN calculation in the interpretation of the weaker features appearing in these spectra.

Path-integral molecular concentration values were obtained using the following procedures. The transmission values shown in Figs. 14 and 15 can be related to absorber concentrations and the path length as follows:

$$T = \exp(-u_L K_L - u_C K_C), \tag{1}$$

where T is the measured transmission, u_L and u_C are the absorber amounts corresponding to line and continuum absorptions, respectively, and K_L and K_C are the corresponding absorption coefficients. Equation (1) can be written as

$$\ln T = -u_L K_L - u_C K_C . \tag{2}$$

Away from an absorption line $K_L = 0$ and the "continuum transmission," T' is related to the product $u_C K_C$ by

$$-\ln T' = u_C K_C . \tag{3}$$

Equation (1) can then be written as

$$\ln (T'/T) = u_L K_L . \tag{4}$$

Now

$$u_L = 7.34 \times 10^{21} \frac{PL}{\theta}, \tag{5}$$

where P is the pressure in atm., L is the path length in cm, and θ is the temperature in K.

The spectral absorption coefficient for a single Lorentz absorption line (true for atmospheric pressures above 0.1 atm.) is given by

$$K_L(\nu) = \frac{S\alpha}{\pi\left[(\nu - \nu_0)^2 + \alpha^2\right]}, \tag{6}$$

where S is the line strength in cm^{-1} per molecule cm^{-2}, α is the collision-broadened half-width in cm^{-1}, ν is the wavenumber in cm^{-1}, and ν_0 is the line center position in cm^{-1}. At line center when $\nu = \nu_0$ Eq. (6) simplifies to

$$K_L = \frac{S}{\pi\alpha}. \tag{7}$$

For the measurements under consideration here, L in Eq. (5) is 6.4 km = 6.4×10^5 cm, and an average representative temperature is 68°F = 293 K. Therefore Eq. (4) can be written as

$$ln(T'/T) = 7.732 \times 10^{21} \frac{S}{\alpha} P, \tag{8}$$

where P is in torr. Equation (8) has been corrected for the WSMR atmospheric pressure of 660 torr.

The line strength values for HDO listed in Refs. 5 and 6 incorporate the HDO/H_2O abundance ratio of 0.03%, therefore, the partial pressure of H_2O corresponding to measurements of the HDO absorption line-center transmission values for the spectra shown in Figs. 14 and 15 is given by

$$P(\text{torr}) = ln(T'/T) \times 1.293 \times 10^{-22} \frac{\alpha}{S}. \tag{9}$$

The usual specification for CH_4 and N_2O concentrations is in parts per million (ppm) and path-integral concentrations of these molecules can be obtained from the long-path WSMR spectra by an analogous relationship as follows:

$$N(\text{ppm}) = ln(T'/T) \times 1.959 \times 10^{-19} \frac{\alpha}{S}. \tag{10}$$

Equation 9 has been used to derive path-integral values for H_2O based primarily on measurements of several strong, well isolated HDO lines and a few relatively weak H_2O absorption lines. Path-integral values for CH_4 and N_2O concentrations have been obtained by using Eq. 10. The results of these analyses for the regions of the three spectra shown in Figures 14 and 15 are contained in Table 5. For the 17 HDO lines measured, average absolute humidity values of 3.69 ± 0.25, 1.38 ± 0.088, and 2.37 ± 0.154 torr, respectively, were obtained for spectra ASL04RN, ASL18RN, and ASL21RN. These values are to be compared to those obtained from the meteorological measurements described in Section 3.3 which are 4.5. 2.0, and 2.5 torr, respectively. The infrared-derived values have a standard deviation of about ±6% of the average value, which is comparable to the values derived from dew-point hygrometer measurements which are usually accurate to about ±0.5°C, corresponding also to ±6% at 4 torr. Considering the combined measurement uncertainty in comparing the two methods of absolute humidity measurement, the values derived from the infrared spectra for the three examples considered here indicate slightly lower values for absolute humidity than do the meteorological measurements. Not much significance should be attached to this observation, however, in light of the assumed HDO/H_2O abundance ratio used in deriving the infrared absolute humidity results.

Additional spectral analysis in other regions where stronger and more numerous H_2O absorption lines exist would be useful in experimentally studying the HDO/H_2O ratio as well as in comparing path-integral and fixed-point sampling values of absolute humidity.

Because only three relatively weak water vapor (161 isotope) lines can be identified in the spectral region analyzed, the relationship of the absolute humidity values obtained from these lines (shown in Table 5(b)) to those obtained from the HDO line analysis (Table 5(a) can be considered fortuitous. In comparisons of H_2O-line-derived absolute humidity values with those derived from the HDO lines, the range of measured values overlaps for each of the three spectra, so that the 0.03% HDO/H_2O abundance ratio appears correct for these comparisons, subject to the several limitations discussed above.

Path-integral values of CH_4 and N_2O derived from the same three spectra are listed in Table 5(b). The CH_4 values vary between 1.77 and 2.73 ppm, which is somewhat larger than the model atmosphere value of 1.6 ppm. An independent point-sampling monitor was used to measure CH_4 concentrations at the ARKY site. It yielded a value of 1.38 ppb [7] for the time during which the 1.77 ppb value was obtained using spectrum ASL04RN.

The N_2O values are greater than the model atmosphere value by about a factor of 10, which is unrealistically high and undoubtedly due to inaccuracies caused by line blending, etc. The qualifications previously stated for analyses of the H_2O line data apply also to analysis of the spectra of these molecules as well, especially for N_2O, since only two very weak relatively isolated lines in this region can be identified near 2773 cm^{-1} and 2779 cm^{-1}. In an attempt to improve the N_2O measurements, additional analysis of spectrum ASL04RN near 2500 cm^{-1} was carried out since a number of stronger absorption lines for this molecule occur in this spectral region. Figure 16 is a high dispersion trace showing several of these lines between 2538 cm^{-1} and 2545 cm^{-1}. Table 6 contains the tabulated data for several lines in this N_2O band, used to derive a value for the path-integrated concentration for spectrum ASL04RN. Column 10 of Table 6 lists the N_2O concentration values in ppm determined from a measurement of each of the lines listed in the table. Based on this

Table 5 — Path-Integral Molecular Absorber Concentrations (a) HDO

Line Position CAL (cm^{-1})	OBS	Species*	α/S (cm^2/mol)	ASL04RN 3-14-79 1630 MST† T	T'	$ln\left(\frac{T'}{T}\right)$	$C^{\ddagger}$	ASL18RN 3-17-79 1652 MST† T	T'	$ln\left(\frac{T'}{T}\right)$	$C^{\ddagger}$	ASL21RN 3-18-79 1700 MST† T	T'	$ln\left(\frac{T'}{T}\right)$	$C^{\ddagger}$
2680.759	2680.70	162	0.124 E 23	0.103	0.832	2.089	3.85	0.308	0.771	0.9176	1.48	0.160	0.790	1.5969	2.56
2689.785	2689.75	162	0.200 E 23	0.232	0.832	1.277	3.80	0.445	0.771	0.5496	1.42				
2692.750	2692.70	162	0.139 E 23	0.130	0.832	1.856	3.84	0.353	0.756	0.7616	1.37	0.217	0.780	1.2794	2.30
2695.208	2695.15	162	0.188 E 23	0.221	0.832	1.326	3.71	0.447	0.765	0.5373	1.30	0.325	0.780	0.8755	2.12
2708.179	2708.15	162	0.237 E 23	0.300	0.820	1.006	3.55	0.507	0.772	0.4205	1.28	0.395	0.783	0.6842	2.09
2716.271	2716.20	162	0.369 E 23	0.390	0.820	0.7432	4.08	0.574	0.758	0.2781	1.33	0.487	0.783	0.4749	2.67
2726.161	2726.10	162	0.183 E 23	0.207	0.820	1.377	3.75	0.425	0.771	0.5956	1.41	0.289	0.780	0.9929	2.35
2730.928	2730.88	162	0.370 E 23	0.415	0.822	0.6835	3.77	0.580	0.771	0.2847	1.36	0.487	0.780	0.4710	2.58
2738.052	2730.05	162	0.655 E 23	0.540	0.820	0.4180	4.08	0.647	0.765	0.1675	1.42	0.593	0.780	0.2741	2.32
2751.342	2751.25	162	0.185 E 23	0.198	0.830	1.433	3.95	0.393	0.768	0.6700	1.61	0.274	0.780	1.0462	2.56
2753.545	2753.50	162	0.138 E 23	0.149	0.830	1.718	3.53	0.349	0.768	0.7887	1.41	0.217	0.775	1.2730	2.27
2764.551	2764.50	162	0.121 E 23	0.120	0.830	1.934	3.48	0.333	0.752	0.8146	1.28	0.179	0.777	1.4681	2.30
2767.277	2767.20	162	0.109 E 23	0.095	0.830	2.168	3.52	0.292	0.763	0.9605	1.35	0.137	0.777	1.7355	2.45
2772.259	2777.20	162	0.134 E 23	0.131	0.820	1.834	3.66	0.323	0.767	0.8648	1.50	0.192	0.760	1.3758	2.39
2777.301	2777.25	162	0.108 E 23	0.110	0.820	2.009	3.29	0.295	0.761	0.9477	1.32	0.138	0.760	1.7061	2.38
2779.969	2779.90	162	0.103 E 23	0.105	0.820	2.055	3.15	0.290	0.761	0.9647	1.28	0.129	0.767	1.7827	2.37
2796.294	2796.25	162	0.175 E 23	0.186	0.780	1.434	3.74	0.404	0.745	0.6120	1.39	0.272	0.770	1.0406	2.39
						AV	3.69				1.38				2.37
							±0.25 torr				±0.088 torr				±0.19 torr

*162 = HDO

†Time of laser extinction measurement used for absolute transmission calibration of FTS spectra.

‡Concentrations of total water vapor based on a 0.03% abundance of HDO/H_2O.

Table 5—Path-Integral Molecular Absorber Concentrations (b) H_2O, CH_4, and N_2O

Line Position CAL	(cm^{-1}) OBS	Species*	α/S (cm^2/mol)	ASL04RN 3-14-79 1630 MST† T	T'	$\ln\left(\frac{T'}{T}\right)$	C	ASL18RN 3-17-79 1652 MST† T	T'	$\ln\left(\frac{T'}{T}\right)$	C	ASL21RN 3-18-79 1700 MST† T	T'	$\ln\left(\frac{T'}{T}\right)$	C
2681.792	2681.75	161	0.309 E 24	0.770	0.832	0.0774	3.56	0.750	0.776	0.0341	1.36	0.745	0.782	0.0485	1.94
2693.335	2693.30	161	0.143 E 24	0.624	0.770	0.2103	4.48	0.686	0.745	0.0825	1.53	0.668	0.766	0.1369	2.53
2732.491	2732.45	161	0.542 E 23	0.535	0.832	0.4416	3.56	0.633	0.775	0.2024	1.42	0.588	0.783	0.2864	2.01
						AV	3.87				1.44				2.16
							±0.531				±0.086				±0.32
							torr				torr				torr
2691.200	2691.15	211	0.196 E 21	0.772	0.810	0.0480	1.84	0.715	0.760	0.0610	2.34	0.725	0.777	0.0693	2.66
2691.590	2691.50	211	0.209 E 21	0.768	0.800	0.0408	1.67	0.715	0.760	0.0610	2.50	0.732	0.777	0.0597	2.44
2757.600	2757.55	211	0.136 E 21	0.703	0.770	0.0910	2.42	0.662	0.738	0.1087	2.90	0.660	0.755	0.1345	3.58
2761.350	2761.30	211	0.131 E 21	0.779	0.815	0.0452	1.16	0.705	0.760	0.0751	1.93	0.707	0.772	0.0880	2.26
						AV	1.77				2.42				2.73
							±0.519				±0.401				±0.58
							ppm				ppm				ppm
2773.457	2773.40	442	0.169 E 21	0.680	0.815	0.0619	2.06	0.693	0.760	0.0923	3.06	0.695	0.765	0.0960	3.18
2795.008	2794.95	442	0.188 E 21	0.737	0.783	0.0605	2.23	0.688	0.747	0.0823	3.03	0.683	0.752	0.0962	3.54
						AV	2.14				3.04				3.36
							±0.120				±0.02				±0.25
							ppm				ppm				ppm

*161 = H_2O, 211 = CH_4, 446 = N_2O.
†Time of laser extinction measurement used for absolute transmission calibration of FTS spectra.

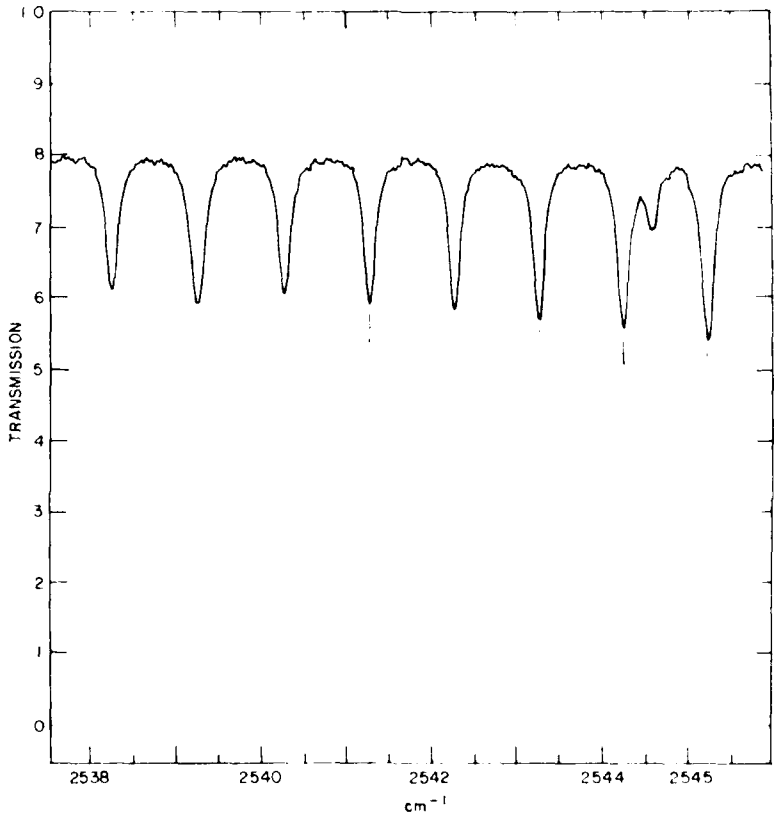

Fig. 16 — High dispersion trace of spectrum ASL04RN 2538 cm^{-1} to 2545 cm^{-1} showing a portion of the band used for the measurement of path-integral N_2O concentration

Table 6 — Path-Integral N_2O Concentration (ASL04RN)

Line Position CAL (cm^{-1})	Line Position OBS (cm^{-1})	T	T'	Species*	S (cm^{-1}/molecule cm^{-2})	α (cm^{-1})	$ln\left(\frac{T'}{T}\right)$	α/S (cm^2/molecule)	C (ppm)
2530.006	2529.85	0.680	0.795	446	6.50 E-21	0.075	0.1562	0.0115 E-21	0.352
2531.071	2531.00	0.690	0.798	446	7.28 E-21	0.075	0.1454	0.0103 E-21	0.293
2535 266	2535 20	0.655	0.798	446	1.09 E-20	0.076	0.1975	0.0697 E-20	0.270
2536.298	2536.22	0.635	0.798	446	1.90 E-20	0.077	0.2285	0.0405 E-20	0.181
2538.343	2538.25	0.612	0.798	446	1.40 E-20	0.077	0.2654	0.0550 E-20	0.286
2540.362	2540.25	0.605	0.798	446	1.61 E-20	0.078	0.2769	0.0484 E-20	0.263
2541.362	2541.27	0.587	0.798	446	1.71 E-20	0.079	0.3071	0.0462 E-20	0.278
2542.355	2542.27	0.585	0.793	446	1.81 E-20	0.079	0.3042	0.0436 E-20	0.260
2543.341	2543.25	0.567	0.792	446	1.90 E-20	0.080	0.3342	0.0421 E-20	0.276
2544.320	2544.22	0.555	0.790	446	1.99 E-20	0.080	0.3531	0.0402 E-20	0.278
2545.293	2545.22	0.541	0.790	446	2.06 E-20	0.081	0.3786	0.0393 E-20	0.291
2551.917	2551.84	0.557	0.800	446	2.18 E-20	0.086	0.3620	0.0394 E-20	0.279
2553.749	2553.70	0.578	0.800	446	2.05 E-20	0.088	0.3250	0.0429 E-20	0.273
2555.554	2555.46	0.597	0.800	446	1.83 E-20	0.090	0.2927	0.0492 E-20	0.282
2558.211	2558.14	0.645	0.807	446	1.34 E-20	0.093	0.2241	0.0694 E-20	0.305
2559.083	2559.97	0.657	0.808	446	1.15 E-20	0.094	0.2069	0.0817 E-20	0.331
2559.948	2559.86	0.675	0.810	446	9.37 E-21	0.094	0.1823	0.0100 E-21	0.357
2567.429	2567.36	0.650	0.806	446	1.80 E-20	0.094	0.2151	0.0522 E-20	0.220
2572.109	2572.05	0.560	0.789	446	2.16 E-20	0.088	0.3428	0.0407 E-20	0.273
2572.865	2572.80	0.545	0.787	446	2.25 E-20	0.087	0.3674	0.0387 E-20	0.278
2574.356	2547.30	0.536	0.789	446	2.37 E-20	0.085	0.3866	0.0359 E-20	0.272
2575.092	2575.00	0.532	0.790	446	2.40 E-20	0.084	0.3954	0.0349 E-20	0.270
2577.966	2577.93	0.535	0.790	446	2.33 E-20	0.081	0.3898	0.0348 E-20	0.266
2583.386	2583.33	0.605	0.800	446	1.59 E-20	0.077	0.2794	0.0484 E-20	0.265
2584.033	2583.96	0.620	0.802	446	1.48 E-20	0.077	0.2574	0.0520 E-20	0.262
								Average	0.278
									±0.034
									(12%)

*446 = N_2O.

analysis, an average value of 0.278 ± 0.034 ppm is obtained, which is in excellent agreement with the model atmosphere value of 0.28 ppm [5].

3.3 Micrometeorological Measurements

The on-site meteorological measurements usually performed by NRL as an integral part of a long-path transmission experiment were not performed during the measurements covered by this report since an existing and continuing atmospheric characterization program was already being carried out by ASL near the optical propagation experiment.

Intensive meteorological measurements in the vicinity of the ARKY hill site were performed by the ASL during part of the long-path transmission measurement times listed in Table 1 (Section 3.1). Complete results of these measurements are contained in Ref. 8. During the optical measurements performed on 12, 16, 17, and 18 March, the ASL measurement system was not in operation and meteorological data acquired at two other sites were used to obtain air temperature, barometric pressure and absolute humidity values for use in the molecular absorption calculations described in Section 4. Each of the two alternate meteorological monitoring stations were approximately 30 km distant from the ARKY hill site, one located at Holloman AFB, the other at WSMR Building 21610. Figure 17 shows the relative locations of the Holloman AFB station, the ARKY hill site, and the WSMR Bldg. 21610 station and their relation to the optical transmission path.

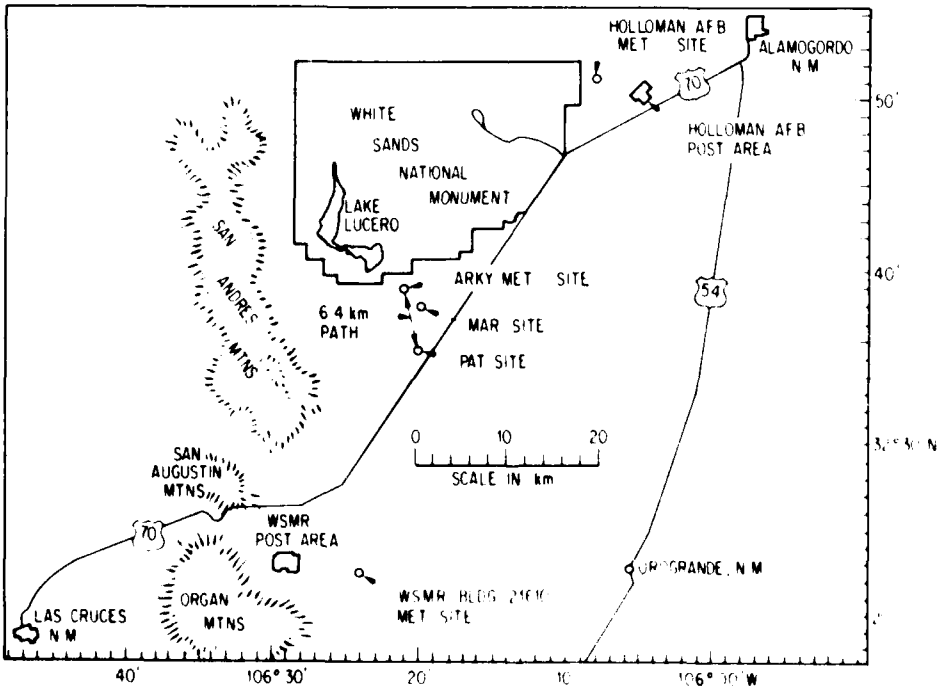

Fig. 17 — Plan view of area surrounding the measurement sites showing the location of the Holloman AFB, ARKY, and WSMR Building 21610 meteorological measurement sites

Table 7 summarizes the pertinent measurements obtained at each of the three meteorological monitoring stations together with values derived from the primary measurements. The derived values are shown in italics in the table.

The WSMR Building 21610 site elevation is slightly lower than the ARKY site and optical path, the former being 1186-m (3925-ft.) while the optical transmitter site at ARKY hill was situated at 1208-m (3965-ft.) elevation. The Holloman AFB site is located at 1246 m (4090 ft.) For cases where data were available concurrently from all three stations, the ARKY site readings are reasonably close to the Holloman station readings and to the Building 21610 values. The values for partial pressure of water vapor shown in Table 7 for the measurement times outside the ASL-ARKY site data base were derived by interpolating between the values measured at the other two sites. The absolute humidity values measured at ARKY are 10-30% lower than those recorded at Holloman. The influence of elevation on the micrometeorology of the local desert environment does not appear to be very large, as demonstrated by the data shown in Table 7. Although the WSMR absolute humidity values appear consistently lower than the ARKY or Holloman readings, they are usually not enough so to be significant, considering the measurement uncertainty of the dew-point measurement apparatus. The importance of continuous on-site meteorological monitoring during optical propagation tests in the WSMR environment is evident from an inspection of the data in Table 7, especially for situations where maximum accuracy in modeling comparisons to the measured data is required.

3.4 Visibility Measurements

Visibility was determined by the contrast method developed by Koschmieder [9-11]. Here visibility is defined as the distance from an object which produces a threshold contrast between the object and the background. In these experiments the target was shadowed mountainside (Elephant Mountain) 33 km away and the background was the sky immediately above the mountain.

The contrast formula is

$$\frac{B_X - B_H}{B_H} = e^{-\alpha X} = T_X \quad \text{(contrast transmittance)}$$

where B_X and B_H are the radiances of the cone of air in front of the target at distance X and the horizon, respectively. The attenuation coefficient α in the visible region can generally be attributed to aerosol scattering. However, in high visibility conditions the molecular component is a significant factor and must be considered in determinations of aerosol effects.

For visibility determination we define γ as the threshold contrast where the target is minimally visible and R as the range at that contrast. For our work we let $\gamma = 0.02$ at a wavelength of 0.55 μm so that

Table 7 — Meteorological Parameters

Date/ Time (MST)	Location	Air Temp. (°F)	Air Temp. (°C)	Dew Point (°F)	Dew Point (°C)	Barometric Press. (mb)	Wind Speed (m/s)	Wind Direction	H_2O (torr)	H_2O (g/m^3)	Visibility (km)
3-8-79	Holl.	73	22.7	26	-3.3		3.1	120	3.2	3.1	
1659	ARKY	77	25				5.0	270	3.0	2.9	114
	WSMR	76	24.4	19	-7.2	873.3	1.5	080	2.7	2.6	
3-9-79	Holl.	63	17.2	33	0.6		6.7	130	4.8	4.8	
1620	ARKY	68	20				2.5	185	3.5	3.4	N/A
	WSMR	68	20	26	-3.3	877.7	7.2	240	3.6	3.5	
3-12-79	Holl.	67	19.4	18	-7.8		2.1	150	2.6	2.5	
1650	ARKY								2.5*	2.4	130
	WSMR	70	16	16	-8.9	880.5	2.6	280	2.4	2.3	
3-13-80	Holl.	70	21.1	28	-2.2		2.1	220	4.0	3.9	
1727	ARKY	68	20				3.5	270	3.3	3.2	140
	WSMR	69	20.6	27	-2.8	883.5	2.1	250	3.7	3.6	
3-14-79	Holl.	65	19.4	34	1.1		6.2	140	5.0	4.9	
1630	ARKY	64	18				8.5	140	4.5	4.5	100
	WSMR	66	18.9	38	3.3	884	6.2	140	5.8	5.7	
3-15-79	Holl.	68	20.0	34	1.1		2.1	160	5.0	4.9	
1700	ARKY	68	20				4.0	140	5.0	4.9	115
	WSMR	67	19.4	40	4.4	881.4	2.1	150	6.3	6.2	
3-16-79	Holl.	71	21.7	31	-0.6		6.2	160	4.5	4.4	
1705	ARKY								3.5*	3.4	168
	WSMR	73	22.2	16	-8.9	875.8	7.7	220	2.4	2.3	
3-17-79	Holl.	67	19.4	16	-8.9		8.2	240	2.3	2.2	
1652	ARKY								2.0*	1.9	46
	WSMR	67	19.4	08	-13.3	872.8	9.3	285	1.7	1.6	
3-18-79	Holl.	60	15.6	20	-6.7		3.1	210	2.8	2.8	
1700	ARKY								3.1*	3.1	151
	WSMR	60	15.6	25	-3.9	876	0.51	190	3.4	3.3	

*Interpolated

$$\frac{B_R - B_H}{B_H} = e^{-\alpha R} = 0.02$$

or visibility = $3.92/\alpha$. An optical pyrometer is a convenient instrument to use for the determination of B_R and B_H. Using a programmable hand calculator, a visibility observation can be made in about one minute. Table 8 summarizes the visibility measurements made during the experiment. Visibility measurements taken at times close to the laser extinction measurement times are included in Table 7 along with other pertinent meteorological data.

4. COMPARISON OF MEASURED AND CALCULATED TRANSMISSION VALUES

Extinction coefficients corresponding to each laser transmission measurement value are tabulated in Table 1, column 6. The next three columns of the table contain values for air temperature, barometric pressure, and partial pressure of water vapor, respectively, corresponding to each of the laser extinction measurement times. The meteorological parameters listed were derived from several sources as discussed in section 3.3.

Molecular absorption coefficient calculations based on the meteorological data in Table 1 were performed for comparison with measured extinction coefficients and are listed in Column 10 of the table. The last column contains the differences between the measured extinction coefficients and the calculated molecular absorption (CMA) values, that is, Column 6 minus Column 10 in Table 1.

Generally the difference values are quite small, indicating in most cases negligible contribution to transmission loss from aerosol scattering. For the majority of the data presented in Table 1, transmission values exceeded 80% and in many cases were greater than 90% for the 6.4-km path. The extinction coefficient α (km^{-1}) is related to transmission T by Beer's law:

$$\ln T = -\alpha z, \text{ or } \alpha = -\frac{\ln T}{Z}, \tag{11}$$

where Z is the path length in km. Since

$$d\alpha = -\frac{1}{Z}\frac{dT}{T}, \tag{12}$$

the relative uncertainty in α given by $d\alpha/\alpha$ resulting from the relative uncertainty in T, dT/T, can be written as

$$\frac{d\alpha}{\alpha} = -\frac{1}{\ln T}\frac{dT}{T}. \tag{13}$$

Table 8 — Visibility Measurements

Date and Time	Transmission for 33 km	α (km^{-1})	Visibility (km)	Normalized FT Spectra
March 5 1000	0.36	0.031	127	
1230	0.34	0.033	120	
1300	0.35	0.032	124	
1600	0.36	0.031	125	
March 6 0830	0.43	0.025	155	
1230	0.46	0.023	168	
1600	0.40	0.028	142	
March 7 0830	0.43	0.026	152	
1200	0.40	0.028	143	
March 8 1000	0.33	0.033	118	
1400	0.33	0.034	116	
1545	0.36	0.031	126	
1645	0.32	0.034	114	
March 12 1520	0.39	0.029	137	
1730	0.37	0.030	130	
March 13 0930	0.32	0.035	112	
1040	0.33	0.034	117	
1210	0.31	0.036	109	
1330	0.34	0.033	118	
1430	0.34	0.036	120	
1605	0.36	0.031	126	
1800	0.45	0.024	161	
March 14 0930	0.21	0.047	84	
1000	0.16	0.056	70	
1230	0.29	0.037	106	
1500	0.32	0.035	113	
1600	0.27	0.040	99	
1630	0.27	0.039	100 ←	ASL04RN, ASL06RN
1730	0.32	0.034	114	
March 15 0630	0.30	0.036	108	
1500	0.24	0.042	92	
1525	0.26	0.040	97	
1615	0.27	0.040	99	
1700	0.32	0.034	115	
1735	0.25	0.041	94	
March 16 1150	0.30	0.037	106	
1320	0.32	0.034	114	
1500	0.29	0.037	105	
1630	0.33	0.034	116	ASL13RN
1715	0.46	0.023	168 ←	ASL14RN
1800	0.45	0.024	162	ASL15RN
March 17 1200	0.32	0.035	113	
1400	0.28	0.038	102	
1500	0.02	0.112	33	ASL17RN, ASL18RN
1700	0.059	0.086	46 ←	ASL19RN
1730	0.21	0.047	84	ASL20RN
March 18 1545	0.44	0.025	158	
1630	0.43	0.026	151	
1720	0.44	0.025	159 ←	ASL22RN, ASL23RN
1745	0.47	0.023	170	

Thus, the relative uncertainty in α equals that in T only when T is 0.367; for larger values of T, a larger relative uncertainty in α results from a given uncertainty in transmission, approaching a factor of 20 times larger when $T = 0.95$.

For the range of transmission values listed in Table 1, the anticipated ±3% uncertainty in T translates into a range of ±9% to ±59% uncertainty in α. The necessity for using a measurement path at least as long as the 6.4-km path used here to obtain a useful measure of absorption for the highly transmitting DF laser lines is emphasized by these considerations.

Figures 18-20 are graphic presentations of the difference values, Column 11 of Table 1. The plots generally lie between 0 and 0.02 km^{-1}, indicating low aerosol scattering. The small negative values apparent for some cases are not highly significant in light of the very high transmission values and correspondingly large uncertainties in α. The anticipated ±3% transmission uncertainty as manifest in the corresponding uncertainty in α is indicated on the plots of difference values in these figures. In three cases, namely 9, 15, and 18 March, there is an indication that the molecular absorption calculations used may be erroneously large due to too large a value of water vapor pressure being used in the calculation. However the observed small negative difference values are not very significant when compared to the uncertainty ranges shown in the figures.

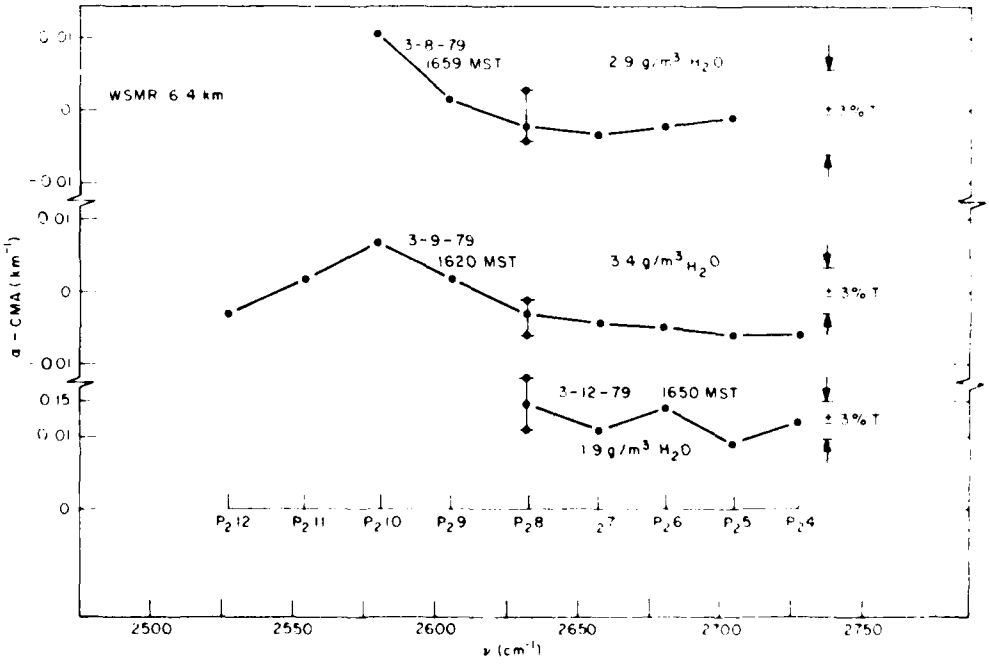

Fig. 18 — Measured extinction coefficient (α) minus calculated molecular absorption (CMA) vs wavenumber for 8, 9, and 12 March 1979

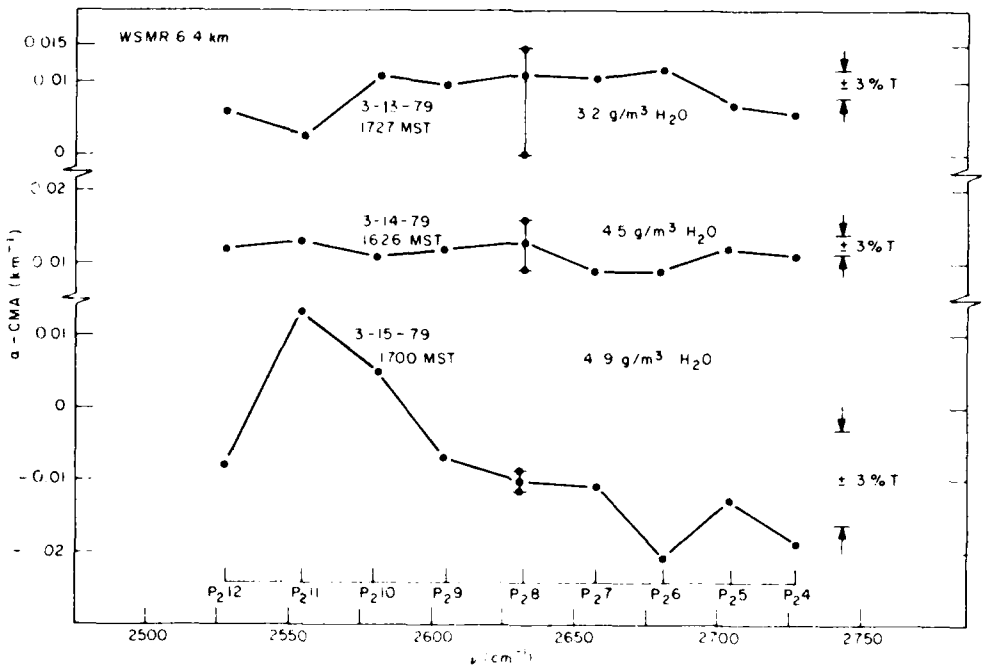

Fig. 19 — Measured extinction coefficient (α) minus calculated molecular absorption (CMA) vs wavenumber for 13, 14, and 15 March 1979

It is anticipated that the difference curves shown in Figs. 18-20 should be independent of wavenumber to within the precision of the measured values. Any nonmolecular attenuation component, i.e., aerosol extinction, is expected to be frequency independent over the spectral interval shown in the figures. For most of the runs shown however, there is a weak trend of decreasing difference values, (α - CMA) with increasing ν, which exceeds the uncertainty ranges shown. The most likely explanation for this effect is that the CMA values are systematically too large for increasing wavenumbers.

The water vapor continuum absorption model of Watkins and White [12] was used in the HITRAN [5] calculation procedure to obtain the CMA values shown in Table 1. Earlier comparisons [13] indicated that the magnitude of the Watkins and White continuum absorption model was generally in agreement with values derived from long-path FTS data for 5-km coastal paths and 12-torr partial pressure of water vapor, but that higher absorption than measured was predicted for increasing wavenumbers between 2600 and 2800 cm^{-1}, especially for larger values of absolute humidity ($\sim$18 torr). While the humidity range encountered in the present experiment is much lower (only 2- to 5-torr partial pressure of water vapor), the same trend is observed as in the earlier comparisons. Recently, additional measurements [14] similar to those reported here were performed over a 4.07-km path at San Nicolas Island, California; analysis of data from this experiment is in agreement with and extends the trends observed in the results of the present experiment to conditions of higher humidity.

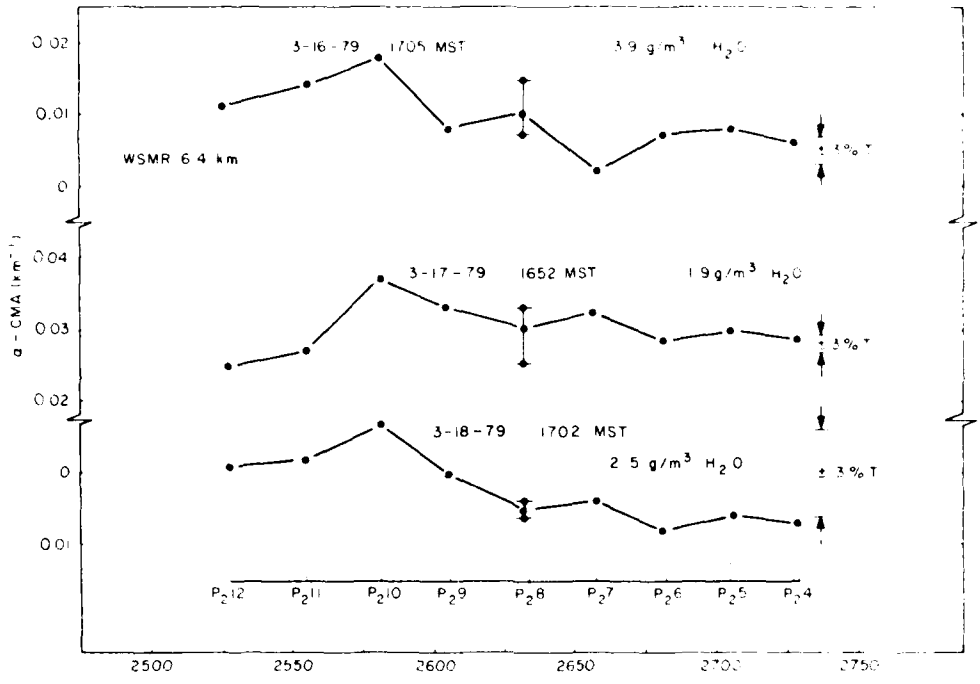

Fig. 20 -- Measured extinction coefficient (α) minus calculated molecular absorption (CMA) vs wavenumber for 16, 17, and 18 March 1979

There is an indication in several of the plots shown in Figs. 18-20 that the difference values obtained for the P2-10 line at 2580.096 cm^{-1} are abnormally large over and above the trend manifested by the remainder of the data points. It has been pointed out in Section 3.2.1 that this laser line is located on the shoulder of an atmospheric N_2O absorption line. The near-coincidence of line centers renders a transmission measurement on this line particularly sensitive to small changes in the DF laser output frequency which may occur due to longitudinal mode shifting within the laser source. The unstabilized laser source has a 1-m optical cavity length, giving a longitudinal mode spacing of 1.5 MHz or about 5×10^{-3} cm^{-1}. A shift in laser output frequency corresponding to a shift in one or two longitudinal modes within the laser cavity could be reflected in a sizeable change in measured transmission for the P2-10 line. Earlier transmission measurements on this line have also shown large amounts of scatter in the data [1,4].

5. CONCLUSIONS AND RECOMMENDATIONS

The results of the experiment described in this report have shown very low aerosol extinction at visible wavelengths at the WSMR site. Visibilities measured with a telepyrometer technique ranged from an isolated "low" value of 33 km to a typical average value of 110 to 120 km with a few high values exceeding 150 km.

The analysis and comparisons contained in Sections 3.1 and 4 show that aerosol contributions to total measured extinction at DF wavelengths are typically no larger than $\sim$0.015 km^{-1}, which is representative of the WSMR location during the late afternoon hours when these measurements were made. The average range of measured visible extinction coefficients tabulated in Table 8 varies between ~0.025 km^{-1} and about 0.04 km^{-1}, which is in the anticipated relationship to the infrared values for the continental aerosol expected in the inland desert.

The set of measurements taken on 15 March appears to be somewhat inconsistent with the remaining data. The absolute humidity of 4.9 g/m^3 recorded on that day was the largest in the experiment, while the measured transmission for the P2-8 DF laser line was 95%, the second highest value observed. Data for the remaining days show a consistent pattern of 82 to 96% measured transmission for the P2-8 line for relatively small amounts of water vapor between 2 and 5 g/m^3. When CMA values are subtracted from the corresponding total extinction coefficients, small apparent aerosol extinction (AAE) values between 0 and 0.018 km^{-1} are obtained which are quite reasonable.

The -0.012 km^{-1} AAE value for 15 March, although unrealistic, is nevertheless a small number in absolute value and not substantially larger than the anticipated experimental uncertainty. Transmission measured for the P2-8 line on 17 March (76%) yielded the largest extinction coefficient observed for this line: 0.042 km^{-1} (average of three readings). When corrected for molecular absorption an average AAE value of 0.033 km^{-1} is obtained, which is about twice the value for the remaining measurements on all other days. Visibility recorded on this day was substantially lower than during the remainder of the experiment, being only 46 km as opposed to the very high visibilities of 100 to 170 km measured otherwise. An inspection of Table 7 shows moderate to high wind speeds moving from SE to SW at the ARKY site for several days prior to 17 March and the highest value of 9.3 m/s from the west recorded by the WSMR building 21610 site on that day. The reduced visibility and greater aerosol extinction at 3.8 μm are a direct consequence of these high wind conditions.

The P2-10 DF laser line consistently showed the largest absorption of any lines measured, with extinction coefficients averaging about 0.060-0.070 km^{-1}. Absorption by atmospheric N_2O is primarily responsible for this attenuation, along with a secondary absorption component due to water vapor (see discussion in Section 3.2). Again the data from 15 March show high transmission for the high value of water vapor, although the measurement for this line with an AAE value of 0.005 km^{-1} is more reasonable than the relatively large negative values obtained for the other lines. The AAE contribution of 0.037 km^{-1} on 17 March for the P2-10 is consistent with the larger aerosol scattering values seen for the other lines on that day.

The measurements described in Section 3.2 of this report demonstrate that very good absolute transmission calibrations of the high resolution FTS data are achievable with residual average transmission scale offsets well below 1% absolute transmission and with a "fitting error" or standard deviation usually less than 0.02 for all but a few "noisy" examples of the spectra.

The limited analysis of a few examples of the calibrated FTS spectra which is presented in Section 3.2 points out the great wealth of information contained within these data and the fundamental role they can play in a detailed characterization of atmospheric composition

and infrared properties in the WSMR environment. Determinations of path average values of HDO and H_2O are shown to be consistent with local dew-point hygrometer measurements of absolute humidity for the cases examined. Spectroscopically derived values for N_2O and CH_4 concentrations agree well with accepted model atmosphere values, but only a very limited analysis has been possible within the scope of the effort covered by this report. Routine collection and utilization of high resolution FTS data based on the procedures and techniques described in this report is highly recommended to continuously and fully characterize the infrared environment at WSMR in support of future infrared systems tests.

The comparisons presented in Section 4 indicate a weak trend in the data showing that molecular absorption calculations done with the Watkins and White water vapor continuum absorption model predict too large an increase in absorption with increasing wavenumber between 2600 and 2800 cm^{-1}. However the weak trends indicated are not highly significant when compared to the range of experimental uncertainties in the measured extinction coefficients for the low-aerosol-scattering, low-water-vapor conditions in this experiment.

In summary, the measurements described in this report provide a representative sampling of atmospheric transmission at DF laser wavelengths for the WSMR location during the low-humidity, high-visibility conditions encountered in the spring season at that location. Earlier experiments of a similar nature were performed during midsummer 1978 (see Ref. 1) during somewhat more humid conditions (at least for the WSMR location). Absolute humidities in that experiment ranged between 4 and 14 g/m^3 H_2O, but measured extinction coefficients were not significantly different from those observed during this experiment. In the earlier experiment AAE values of $\sim \pm 0.005$ km^{-1} were consistently observed, with visibilities always greater than 120 km.

Transmission measurements during the March 1979 experiment extended over twice as many days as in the earlier experiment; however, in each case only a limited sampling of conditions was possible within experimental and programmatic constraints. Nevertheless, a reasonably valid comparison of atmospheric propagation characteristics at the WSMR location for the two seasons of the year has been obtained in these experiments. During the days in the August 1978 experiment when long-path transmission data were taken, wind conditions were consistently moderate between 1.2 and 4.5 m/s. The higher humidity and generally wetter conditions at that time resulted in lower airborne particulate extinction at infrared wavelengths than in the Spring 1979 experiment. Increased molecular absorption at DF laser frequencies due to the higher atmospheric water vapor together with lower aerosol scattering in August 1978 resulted in about equivalent transmission loss in each experiment. In the August 1978 experiment, contributions due to aerosol scattering were very low, consistently less than 0.005 km^{-1}, while they were about three times this value during March 1979. During the later experiment, molecular absorption at the P2-8 DF line ranged between 0.010 and 0.018 km^{-1} (excepting the data from 15 March), which is about 60% of the range of values measured during the previous summer. The relative importance of aerosol scattering and molecular absorption is seen to be interchanged when comparing the measurements from the two experiments.

Since only a single CO_2 laser transmission measurement was possible during the second experiment, no meaningful conclusions can be drawn which are consistent with the observations cited above regarding transmission at DF laser wavelengths. The CO_2 laser transmission

data contained in the report of the earlier experiment (Ref. 1) must suffice until further measurements can be accomplished at the WSMR site.

6. ACKNOWLEDGMENTS

The authors wish to thank Mr. Glenn Hoidale of the Army ASL for help in support of this project, for assistance in obtaining and interpreting the meteorological data presented in Section 3.3, and for additional helpful suggestions in preparing this report. They also wish to express their thanks to Dr. Donald Walters, ASL, and Dr. William Guttman, Optimetrics, Inc., for use of and assistance with the ASL MIDAC 1000 FTS system, used for part of the reduction of the data.

The technical support of the Navy HEL office at WSMR, particularly from Senior Chiefs W. Moore, G. Oakley, and J. Jacques, was particularly helpful in contributing to a successful experiment. Technical assistance supplied by F. Tidball and technical discussions with D. Leslie, Sachs-Freeman Associates, are greatly appreciated.

The authors are grateful to C. Acton for the preparation of the many photographic records in this report and are especially grateful to Mrs. Nell Grimley for her patient and dedicated typing, including the many extensive tables.

REFERENCES

1. S. T. Hanley, J. A. Dowling, R. F. Horton, J. A. Curcio, C. O. Gott, M. Woytko, and J. Storvick, "Atmospheric Transmission Measurements at White Sands Missile Range, August 1978," NRL Report 8422, July 1980.
2. J. A. Dowling, R. F. Horton, G. L. Trusty, T. H. Cosden, K. M. Haught, J. A. Curcio, C. O. Gott, S. T. Hanley, P. B. Ulrich, and W. L. Agambar, "Atmospheric Transmission Measurement Program and Field Test Plan," NRL Report 8059, November 30, 1977.
3. T. H. Cosden, J. A. Curcio, J. A. Dowling, C. O. Gott, D. H. Garcia, S. T. Hanley, K. M. Haught, R. F. Horton, G. L. Trusty, and W. L. Agambar, "Atmospheric Transmission Measurement Program Report for 1 July through 30 September 1976 (TQ1976)," NRL Report 8104, September 1, 1977.
4. J. A. Dowling, K. M. Haught, R. F. Horton, G. L. Trusty, J. A. Curcio, T. H. Cosden, S. T. Hanley, C. O. Gott, and W. L. Agambar, "Atmospheric Extinction Measurements at Nd-YAG and DF Laser Wavelengths Performed in Conjunction with the JAN Propagation Tests, June-September 1975," NRL Report 8058, February 10, 1978.
5. R. A. McClatchey, W. S. Benedict, S. A. Clough, D. E. Burch, R. F. Calfee, K. Fox, L. S. Rothman, and J. S. Garing, "AFCRL Atmospheric Line Parameters Compilation," Report AFCRL-TR-73-0096 (Air Force Cambridge Research Laboratories, Hanscomb AFB, Mass.), 1973.
6. L. S. Rothman, "Update of the AFGL Atmospheric Absorption Line Parameters Compilation," Appl. Opt. 17, 3517 (1978).

7. W. Flowers, D. McCullough and G. Hoidale, "Atmospheric Gases at the High Energy Laser System Test Facility (HELSTF) White Sands Missile Range (WSMR), New Mexico, January to October 1979," U.S. Army Electronics Research and Development Command, Atmospheric Sciences Laboratory, WSMR, New Mexico (in preparation).

8. D. McCullough, et al, "Atmospheric Conditions at the High Energy Laser System Test Facility (HELSTF), White Sands Missile Range (WSMR), New Mexico 7 to 9 and 13 to 15 March 1979," U. S. Army Atmospheric Sciences Laboratory (ASL) Report ASL-DR-79-003, ASL-WSMR, New Mexico 88002 (November 1979).

9. W. E. K. Middleton, *Vision Through the Atmosphere*, Toronto: University of Toronto Press (1952).

10. J. A. Curcio and G. L. Knestrick, "Atmospheric Transmission Measurements with an Optical Pyrometer," (Abst.) J. Opt. Soc. Am. 47, 113 (1957).

11. J. A. Curcio and K. A. Durbin, "Atmospheric Transmission in the Visible Region," NRL Report 5368, October 1959.

12. W. R. Watkins and K. O. White, Opt. Ltrs. 1, 31 (1977).

13. J. A. Dowling, R. F. Horton, S. T. Hanley, and K. M. Haught, "High Resolution Field Measurement of Atmospheric Transmission," SPIE Proc. 142, 25 (1978).

14. J. A. Dowling, S. T. Hanley, J. A. Curcio, C. O. Gott, F. A. Tidball, G. B. Matthews, and A. Ackermann, "Results of Laser-Calibrated High-Resolution Transmission Measurements and Comparisons to Broadband Transmissometer Data: San Nicolas Island, California, May 1979," NRL Report to be published.